

A LABORATORY STUDY OF THERMAL CONVECTION
UNDER A CENTRAL FORCE FIELD

BY

BHUVANESH CHANDRA

B.Sc., University of Lucknow, 1961
M.Sc., Indian Institute of Technology, Kharagpur, 1965
M.Sc., University of Western Ontario, 1969

A THESIS SUBMITTED IN PARTIAL FULFILMENT OF
THE REQUIREMENTS FOR THE DEGREE OF
DOCTOR OF PHILOSOPHY
in the Department
of
GEOPHYSICS

We accept this thesis as conforming to the
required standard

THE UNIVERSITY OF BRITISH COLUMBIA

November, 1971

In presenting this thesis in partial fulfilment of the requirements for an advanced degree at the University of British Columbia, I agree that the Library shall make it freely available for reference and study.

I further agree that permission for extensive copying of this thesis for scholarly purposes may be granted by the Head of my Department or by his representatives. It is understood that copying or publication of this thesis for financial gain shall not be allowed without my written permission.

Department of Geophysics

The University of British Columbia
Vancouver 8, Canada

Date December 27, 1971.

ABSTRACT

This thesis presents the results of a theoretical and experimental study of thermal convection under the influence of a central force field. Flows in the atmosphere and in the core of the earth are thought to occur under a near balance between Coriolis and buoyancy forces. Thus, a desirable model of these flows would include spherical symmetry in the force field and rotation. The present study, in which convection under a central force field in cylindrical geometry has been achieved, is the first step towards such a model.

The system consists of a cool outer cylinder and a hot inner cylinder with a dielectric liquid (silicone oil) filling the annulus between them. The common axis of the cylinders is vertical. The inner cylinder is grounded and the outer cylinder is kept at a high alternating (60 Hz) potential. This intense alternating electric field provides the radial buoyancy force which results in convective heat transfer at a certain critical temperature gradient.

The fluid in the system is found to behave like a layer of fluid in a gravitational field, heated from below. Below a certain critical value of a dimensionless number (equivalent to

(11)

the Rayleigh number with the electrical force substituted for gravity) there is no convective heat transfer. Above the critical value, flow sets in with the convective heat transfer proportional to the modified Rayleigh number. Marginal stability analysis gives a critical electrical Rayleigh number in agreement with the experimentally determined value.

TABLE OF CONTENTS

ABSTRACT	(i)
LIST OF FIGURES	(v)
LIST OF TABLES	(vii)
ACKNOWLEDGEMENTS	(viii)
CHAPTER I GENERAL INTRODUCTION	
1.1 Introduction	1
1.2 Thermal convection and geophysical applications	4
1.3 Scope of this thesis.	7
CHAPTER II THEORY	
2.1 Introduction	9
2.2 The perturbation equations	11
2.3 The principle of exchange of stabilities	23
2.4 The solution for the case of a narrow gap	27
2.5 The solution for a wide gap when the marginal state is stationary	28
CHAPTER III EXPERIMENTAL ARRANGEMENT AND RESULTS	
3.1 Introduction	37
3.2 Experimental arrangement	40
3.3 The experimental procedure	48

3.4	Errors and corrections	54
3.5	The experimental results	63
3.6	Accuracy	65
CHAPTER IV DISCUSSION AND CONCLUSIONS		
4.1	Discussion of results	66
4.2	Conclusions	67
REFERENCES		68
APPENDIX I TABLES OF THERMISTOR CALIBRATION		71
APPENDIX II TABLES OF HEAT TRANSFER MEASUREMENTS		74
APPENDIX III TABLES OF CORRECTED DATA		83

LIST OF FIGURES

FIGURE 1	Coordinate system and cylindrical cavity.	10
FIGURE 2	Dependence of the numerically determined electrical Rayleigh number on the dimensionless wave number.	32
FIGURE 3	The velocity profile.	33
FIGURE 4	The temperature profile.	34
FIGURE 5	The stream lines at the onset of instability.	35
FIGURE 6	A cross section of the apparatus.	39
FIGURE 7	The circuit for the heating coil.	41
FIGURE 8	Circuit for the bridge.	44
FIGURE 9	Kinematic viscosity as a function of temperature.	45
FIGURE 10	Dielectric constant as a function of temperature.	46
FIGURE 11	Dependence of the temperature of the outer cylinder less mean of inlet-outlet temperatures on heat transfer rate.	49
FIGURE 12	Calibration of Ammeter I_1 against a laboratory standard.	51
FIGURE 13	Calibration of ammeter I_2 against a laboratory standard.	52
FIGURE 14	Calibration of voltmeter against a laboratory standard.	53
FIGURE 15	Dependence of temperature difference on heat transfer rate for 0 kv rms between the cylinders.	55
FIGURE 16	Dependence of temperature difference on heat transfer rate for 4.06 kv rms between the cylinders.	56

FIGURE 17	Dependence of temperature difference on heat transfer rate for 6.00 kv rms between the cylinders.	57
FIGURE 18	Dependence of temperature difference on heat transfer rate for 6.92 kv rms between the cylinders.	58
FIGURE 19	Dependence of temperature difference on heat transfer rate for 7.91 kv rms between the cylinders.	59
FIGURE 20	Dependence of temperature difference on heat transfer rate for 9.63 kv rms between the cylinders.	60
FIGURE 21	Dependence of temperature difference on heat transfer rate for 10.15 kv rms between the cylinders.	61
FIGURE 22	Dependence of temperature difference on heat transfer rate for 10.80 kv rms between the cylinders.	62
FIGURE 23	Nusselt number as a function of electrical Rayleigh number.	64

LIST OF TABLES

Table 1	Electrical body force at the inner and outer cylinders for given voltages across the gap.	22
Table 2	Dimensions of the cell.	42
Table 3	Thermistor calibrations for the inner cylinder.	72
Table 4	Thermistor calibrations for the inlet and outlet points.	73
Table 5	Typical properties of silicone oil.	48
Table 6	Observed data at 0 kv rms.	75
Table 7	Observed data at 4.06 kv rms.	76
Table 8	Observed data at 6.00 kv rms.	77
Table 9	Observed data at 6.92 kv rms.	78
Table 10	Observed data at 7.91 kv rms.	79
Table 11	Observed data at 9.63 kv rms.	80
Table 12	Observed data at 10.15 kv rms.	81
Table 13	Observed data at 10.80 kv rms.	82
Table 14	Corrected data for 0 kv rms.	84
Table 15	Corrected data for 4.06 kv rms.	85
Table 16	Corrected data for 6.00 kv rms.	86
Table 17	Corrected data for 6.92 kv rms.	87
Table 18	Corrected data for 7.91 kv rms.	88
Table 19	Corrected data for 9.63 kv rms.	89
Table 20	Corrected data for 10.15 kv rms.	90
Table 21	Corrected data for 10.80 kv rms.	91

ACKNOWLEDGEMENTS

The author is indebted to Dr. D. E. Smylie for directing the research reported in this thesis. The following persons read the thesis critically: Dr. D. E. Smylie, Dr. G. K. C. Clarke and DR. T. J. Ulrych, all of the Geophysics Department, and Dr. P. H. LeBlond of the Institute of Oceanography. Mr. H. Lau of the Mechanical Engineering Department contributed to many discussions.

Finally, the author wishes to acknowledge the assistance of the staff members and the graduate students of the department who contributed in various capacities.

The work was financed by grants from the National Research Council of Canada to Dr. D. E. Smylie.

CHAPTER I

GENERAL INTRODUCTION

1.1 Introduction

In the last few decades, efforts have been made to study motions in the Earth's atmosphere, oceans, mantle and core through the use of laboratory models (Fultz, 1961; Long, 1954). The incentive for the use of models comes from the difficulties of solving the equations of motion for general convective flow problems. At the present time, the equations governing the general flows can only be solved approximately under idealized conditions. Thus, laboratory models have become important in geophysical fluid dynamics.

The large scale circulation of the atmosphere occurs under the combined influence of a spherically symmetric gravitational field and the rotation of the Earth. It is suspected that a roughly similar situation prevails in the Earth's liquid core. Thus, a laboratory model of these flows should include both the spherical symmetry of the gravitational field and the rotation of the Earth. The effect of rotation has been the subject of study of many authors (for recent references, see Greenspan, 1968). In these studies certain flow regimes have been recognized which seem to have their counterpart in the atmosphere in the form of large scale eddies or cyclones. However, no laboratory model which simulates a spherically symmetric

gravitational field has yet been developed. In the absence of a suitable method of simulating a gravitating fluid sphere in the laboratory, the validity of the rotating models is limited to the polar regions where strong Coriolis forces are present as in the core and the atmosphere. In the thin shell of the atmosphere, however, this defect is not so serious because the flow is essentially two dimensional as opposed to the core flow which is three dimensional.

This thesis is the outcome of a preliminary investigation for setting up a laboratory model of gravitational convection. Smylie(1966) first suggested the use of strong electric field gradients in dielectric liquids to simulate the central nature of the gravitational field. The electrical properties of a liquid are functions of temperature. For a nonpolar liquid the variation of dielectric constant with temperature is due solely to the change in density (Debye, 1929, p 27). Thus, in the presence of temperature variations in the dielectric liquid, an intense electric field results in a buoyancy force. This buoyancy force will produce an instability in the fluid. However, the viscosity, thermal conductivity and the boundaries will act to stabilize the fluid and significant convective heat transfer should occur only when the temperature gradient is appreciable.

In dielectric liquids of moderate dielectric constant, the thermal convection produced by the electric buoyancy force is analogous to gravitational convection, where the instability occurs as a result of heating from below (or cooling from above). In contrast to the ubiquitous

and unalterable gravitational field, however, electric fields can easily be generated and shaped in the laboratory by existing techniques.

In a steady electric field space charges accumulate even in a good dielectric and the circulation of the liquid is due to the movement of these charges. The free charge buildup occurs exponentially in time with a time constant ϵ/σ where ϵ is the permittivity and σ is the conductivity of the fluid. This constant is known as the electrical relaxation time. If an alternating field is applied at a frequency much higher than the reciprocal of the relaxation time, free charge does not have time to accumulate. Thus, in an alternating field, the dielectric effects dominate the free charge effects. The electric body force depends on the gradient of the square of the electric field. For most dielectric liquids (for example, transformer oil and silicone oil), 60 Hz is a sufficiently high frequency to prevent the buildup of free charge. At the same time, dielectric loss at 60 Hz is so low that it makes no significant contribution to the temperature field. Further, variations in the body force are so rapid that its mean value can be assumed in determining fluid motions, except in the case of liquids of extremely low viscosity.

Both theoretical and experimental study of electroconvection (convection under steady fields) has been reported by many authors (for example, Kronig and Schwarz, 1949; Turnbull, 1968; Malkus and Veronis, 1961; Melcher and Taylor, 1969; etc.). The electroconvective

instability occurs even in the absence of temperature variations; Avsec and Luntz (1937) have observed two dimensional toroidal motions in a dielectric liquid filling the gap between two concentric cylinders. When the inner cylinder is earthed and the electrical potential of the outer cylinder is raised, then at some critical potential difference, steady cellular patterns are formed in the fluid.

Recently, Gross(1967) and Gross and Porter(1966) have suggested the use of space charge effects in modelling geophysical flows. In these models, charge transport becomes the analogue of heat transfer and if temperature gradients are present, heat will be advected by the charge induced flow. The mechanisms of charge generation and transfer at the electrodes, and the nature of the process by which charge motion stirs the fluid are not well understood. Therefore, the quality of analogy to geophysical phenomena is not clear.

1.2 Thermal convection and Geophysical applications:

Although the phenomena of thermal convection as a mode of heat transfer was discovered in the 18th century, the first quantitative experiments on convection were done by Bénard(1900). He found that if a thin layer of liquid, free at its upper surface, is heated uniformly at the lower surface, a regime of polygonal convection cells is formed as soon as a certain critical temperature gradient is reached. The walls of these cells are vertical and the movement of the liquid is upward in the centre and downward at the periphery.

Rayleigh(1916) laid the theoretical foundation for the explanation of Bénard's results. It appears now, however, that the convection in Bénard's experiments was actually partially driven by the variations in the free surface conditions and not entirely by the buoyancy forces as Rayleigh assumed. In later experiments (see for example Chandra, 1938; Schmitd and Milverton, 1935; and Silveston, 1958), the free surface has been eliminated by placing an isothermal lid on top of the fluid layer. These experiments also showed the development of regular hexagonal cell patterns. The critical temperature gradient at which convection cells develop increases rapidly as the layer becomes thinner. Several modifications of Rayleigh's theory (for example, Jeffreys, 1926; Pellew and Southwell, 1940; Low, 1929; etc.) to fit this case give excellent agreement with the experimental observations. Rayleigh's approach to the problem (infinitesimal perturbations on an equilibrium state) still remains the basis of the modern treatment of the marginal stability problems (Chandrasekhar, 1961, chapter 2).

It is believed that many flows of geophysical interest are driven by thermal convection. It has been suggested that large scale convection currents exist in the Earth's mantle in attempts by many authors to interpret certain topographic features of the Earth's surface (Vening-Meinesz, 1962). Recently, McFadden(1969) has considered the effect of a region of low viscosity on thermal convection in the Earth's mantle to try to explain how convection

in only the upper mantle could lead to flows of continental horizontal scale.

The presence of thermal convection in the atmosphere was suggested by Hadley (1735); differential heating between different latitudes gives rise to ascent of air in tropical regions. This leads to a flow of air towards the equator at lower levels and a flow away from the equator at higher levels. The combined effects of surface friction and the rotation of the earth deflects these currents and thus, according to Hadley's original theory, easterly winds form at lower levels and westerlies at higher levels. From this idea, the well known cellular model for the circulation of the whole atmosphere has been derived (Rossby, 1941).

The geomagnetic field is now considered to originate from electric currents produced by inductive interaction between hydrodynamical motions in the Earth's conductive fluid core and a small adventitious magnetic field. Thus, a satisfactory theory for the Earth's magnetism requires a satisfactory theory for the hydrodynamics of the core. Several speculations have been made regarding the energy source that drives the fluid motions in the core. Among them thermal convection is one of the possibilities (Bullard and Gellman, 1954).

Oceanographers have long studied the circulation of the oceanic currents. The ocean currents are believed to be the result of the combined effects of the thermohaline motions (density inhomogeneity caused by temperature and/or salinity differences) and the wind driven motions. The former are thought to be more important

in deep water. However, unlike the case of the atmosphere, the thermal convection in the oceans occurs, not because of heating from below, but because of cooling from the upper surface. The thermohaline circulation originates as a vertical flow sinking to mid-depth or even to the ocean bottom, followed by horizontal motion.

1.3 Scope of the present work

This thesis is intended to demonstrate the feasibility of using an intense alternating electric field acting on a dielectric liquid to produce a spherically symmetric force field. A buoyancy force is produced by the variation of dielectric constant with temperature. Since it is a feasibility study, the experiment was set up in cylindrical geometry to simplify construction. However, the techniques learned here can be carried directly over to the spherical case, which is the real geometry for large scale geophysical flows.

The system consists of two vertical concentric cylinders of radii r_1 and r_2 ($r_2 > r_1$). The space between the cylinders is filled with a dielectric liquid (silicone oil). The inner cylinder is maintained at a fixed temperature T_1 which is higher than the constant temperature T_2 of the outer cylinder. In addition to a temperature gradient, a radial, alternating electric field is also imposed between the cylinders.

In chapter II, the marginal stability equations for this

problem are derived under the assumptions of the Boussinesq approximation. The effect of the Earth's gravity has been ignored for this theory. The solution of the marginal stability equations has been found numerically and it is shown that the convection induced by the electrical body force occurs only when the dimensionless number (equivalent to the Rayleigh number with the electric buoyancy force substituted for gravity) exceeds a certain critical value. When the gap thickness is very much smaller than the mean radius of the cylinders (in this limiting case boundaries take the form of plane surfaces rather than cylindrical surfaces), the marginal stability equations are shown to reduce to the case of the Bénard-Rayleigh instability.

In chapter III, the experimental arrangement, technique and results of electrically induced convection in a vertical annulus are described. The onset of thermal convection was detected by heat transfer and temperature measurements. The final experimental results are shown in the form of a graph of the Nusselt number against the electric Rayleigh number.

The study is summarized in the final chapter.

CHAPTER II

THEORY

2.1 INTRODUCTION

The problem to be studied is the thermal convection occurring under the electrical body force in the enclosed annular region formed by two vertical concentric cylinders of radii r_1 and r_2 ($r_1 < r_2$). This geometry is shown in figure 1. Conventional cylindrical coordinates (r, θ, z) are indicated with z vertically upwards.

The inner wall of the cylindrical cavity is held at a fixed temperature T_1 which is greater than the constant temperature T_2 of the outer wall. In addition to a temperature difference, there is also an alternating difference of electrical potential between the cylinders.

In the absence of any temperature variations, an electric body force is produced in the liquid, and in an equilibrium situation, this body force is entirely balanced by the generation of a pressure gradient (Landau and Lifshitz, 1960, pp. 64-69). The presence of temperature variations in the liquid results in buoyancy forces whereby warmer liquid has a tendency to seek regions of less intense electric field, cooler liquid has a tendency to seek regions of more intense electric field. However, this natural tendency on the part of the fluid will be inhibited by its own viscosity. Thus, if the temperature difference

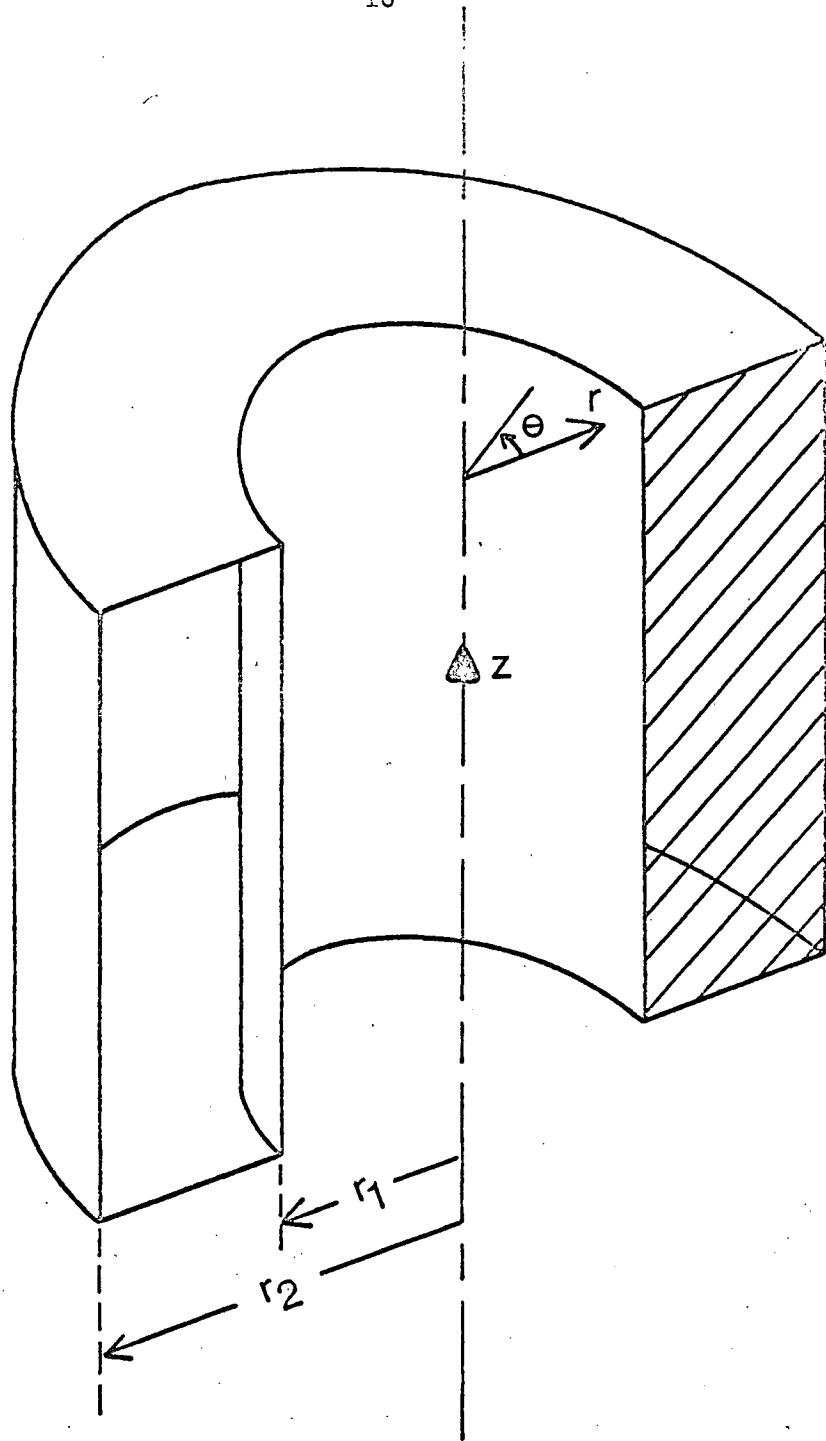


FIGURE 1. CO-ORDINATE SYSTEM AND THE CAVITY.

between the vertical bounding walls is sufficiently small, the heat supplied at the inner wall is transferred to the outer wall by conduction alone. For greater temperature differences, the electric buoyancy force is sufficient to overcome viscous dissipation and the fluid assumes a convective motion. In other words, we expect that the temperature difference between the cylinders must exceed a certain minimum value before convective heat transfer is realized.

The problem under consideration, then, is to solve the marginal stability equations for an incompressible fluid layer bounded by vertical cylindrical walls at different temperatures, in the presence of a radial electrical buoyancy force.

2.2 The Perturbation Equations

The following simplifying assumptions are made in deriving the perturbation equations:

- (1) The fluid is incompressible and the density constant, except as it modifies the electric buoyancy force term.
- (2) The mean square electric field and the temperature distribution in the annulus are functions of radius only.
- (3) The cylinders are of infinite extent, so that the end effects can be ignored.
- (4) The motion is slow and the components of velocity are small enough so that in a first approximation, their products and squares can be neglected.

- (5) The kinematic viscosity and the diffusivity of the fluid are true constants.
- (6) The various perturbations are axi-symmetric and thus independent of θ .
- (7) In deriving the marginal stability equations, the effect of the earth's gravitational field can be ignored. Strictly speaking it is not so. Batchelor (1954) showed that in a narrow cavity between vertical boundaries at different temperatures, there is a slow vertical flow but the heat transfer across the cavity is due mostly to conduction. Thus, the present problem is unstable for all temperature gradients since the earth's gravity is always present. The maximum Grashof number involved in the experiment (described in the next chapter) was about 7.5. This is roughly 10^3 times less than the Grashof number at which free convection sets in (Vest and Arpaci, 1969). The gravity induced flow is likely to be very small at the Grashof number involved in the experiment. It would be an important generalization to carry through a solution taking into account the interaction of the convection induced by the electrical forces with the vertical gravitational base flow, but this difficult problem has not been tackled here.

Consider that initially there are no motions. Thus, the initial

state is characterized by

$$\begin{aligned}\vec{U} &= 0 \\ T &= T(r)\end{aligned}\quad (1)$$

where \vec{U} is the velocity vector and T is the temperature.

In the absence of any motions, the hydrostatic equation reads

$$-\text{grad } p_0 + \vec{f}_0 = 0 \quad (2)$$

where \vec{f}_0 is the electric body force per unit volume at density ρ_0 and temperature T_0 ; p_0 is the pressure distribution.

The temperature distribution is governed by the equation

$$\frac{d}{dr} \left(r \frac{dT_0}{dr} \right) = 0 \quad (3)$$

The solution of equation (3) appropriate to the boundary conditions gives

$$\frac{dT_0}{dr} = - \frac{T_1 - T_2}{\ln \frac{r_2}{r_1}} \cdot \frac{1}{r} \quad (4)$$

The solution for the electric field distribution E_0 is

$$\vec{E}_0 = (E_0, 0, 0), \quad (5)$$

$$E_0 = \frac{V_0}{\ln \frac{r_2}{r_1}} \cdot \frac{1}{r} \quad (6)$$

where V_0 is the root mean square value of the applied potential difference.

Let the perturbed state be characterized by the velocity components

$$U_r, U_\theta, U_z, \quad (7)$$

$$\text{body force } \vec{f} = \vec{f}_0 + \vec{f}', \quad (8)$$

$$\text{density } \rho = \rho_0 + \rho', \quad (9)$$

$$\text{electric field } \vec{E} = \vec{E}_0 + \vec{E}', \quad (10)$$

$$\text{temperature } T = T_0 + T', \quad (11)$$

$$\text{and pressure } p = p_0 + p',$$

primes indicating flow induced quantities.

The general equation for the body force resulting from electric fields in fluid dielectrics is developed by Landau and Lifshitz (1960,p.68). They showed that in an uncharged fluid dielectric of uniform composition, the electric body force per unit volume is given by

$$\vec{f}_0 = 1/2 \rho_0 \text{grad} [E_0^2 \left(\frac{\partial \epsilon}{\partial \rho} \right)_{T_0}] - 1/2 E_0^2 \left(\frac{\partial \epsilon}{\partial T} \right)_{\rho_0} \text{grad } T_0, \quad (12)$$

where ϵ is the electric permittivity of the fluid.

In the perturbed state at temperature T and density ρ , the body force per unit volume is

$$\vec{f} = 1/2 \rho \text{grad} [E^2 \left(\frac{\partial \epsilon}{\partial \rho} \right)_T] - 1/2 E^2 \left(\frac{\partial \epsilon}{\partial T} \right)_\rho \text{grad } T \quad (13)$$

The permittivity of a substance is a function of density and temperature. If the perturbations are small, the permittivity at temperature T and density ρ can be expressed in terms of permittivity at the reference temperature T_0 and density ρ_0 by writing a Taylor expansion. Thus,

$$\begin{aligned} \epsilon(\rho, T) = & \epsilon(\rho_0, T_0) + \left(\frac{\partial \epsilon}{\partial \rho} \right)_{T_0} \rho' + \left(\frac{\partial \epsilon}{\partial T} \right)_{\rho_0} T' \\ & + 1/2 \left[\left(\frac{\partial^2 \epsilon}{\partial \rho^2} \right)_{T_0} \rho'^2 + 2 \left(\frac{\partial^2 \epsilon}{\partial \rho \partial T} \right)_{\rho_0, T_0} \rho' T' + \left(\frac{\partial^2 \epsilon}{\partial T^2} \right)_{\rho_0} T'^2 \right] \\ & + \text{higher order terms} \end{aligned} \quad (14)$$

Therefore, we can write

$$\left(\frac{\partial \epsilon}{\partial \rho} \right)_T = \left(\frac{\partial \epsilon}{\partial \rho} \right)_{T_0} + \left(\frac{\partial^2 \epsilon}{\partial \rho^2} \right)_{T_0} \rho' + \left(\frac{\partial^2 \epsilon}{\partial \rho \partial T} \right)_{\rho_0, T_0} T'$$

and

$$\left(\frac{\partial \epsilon}{\partial T} \right)_\rho = \left(\frac{\partial \epsilon}{\partial T} \right)_{\rho_0} + \left(\frac{\partial^2 \epsilon}{\partial T^2} \right)_{\rho_0} T' + \left(\frac{\partial^2 \epsilon}{\partial \rho \partial T} \right)_{\rho_0, T_0} \rho' \quad (15)$$

Combining (8), (12), (13) and (15), we get to first order in the flow-induced quantities,

$$\begin{aligned} \vec{f}^{\vec{t}} = & 1/2 \rho' \text{grad}[E_0^2 \left(\frac{\partial \epsilon}{\partial \rho} \right)_{T_0}] - 1/2 E_0^2 \left(\frac{\partial \epsilon}{\partial T} \right)_{\rho_0} \text{grad} T' \\ & + \rho_0 \text{grad}[(\vec{E}_0 \cdot \vec{E}') \left(\frac{\partial \epsilon}{\partial \rho} \right)_{T_0}] - (E_0^{\vec{t}} \cdot \vec{E}') \left(\frac{\partial \epsilon}{\partial T} \right)_{\rho_0} \text{grad} T_0 \\ & + 1/2 \rho_0 \text{grad}[E_0^2 \{ \left(\frac{\partial^2 \epsilon}{\partial \rho^2} \right)_{T_0} \rho' + \left(\frac{\partial^2 \epsilon}{\partial \rho \partial T} \right)_{\rho_0, T_0} T' \}] \\ & - 1/2 E_0^2 \left[\left(\frac{\partial^2 \epsilon}{\partial T^2} \right)_{\rho_0} T' + \left(\frac{\partial^2 \epsilon}{\partial \rho \partial T} \right)_{\rho_0, T_0} \rho' \right] \text{grad} T_0 \end{aligned} \quad (16)$$

Chandra (1969) showed that for a fluid dielectric of moderate dielectric constant, the flow-induced changes in the electric field can be neglected. The order of magnitude of the second density and temperature coefficients of permittivity for fluids is very small and can also be taken to be zero. Thus, the electric buoyancy force per unit volume can be written as

$$\vec{f}' = 1/2 \rho' \left(\frac{\partial \epsilon}{\partial \rho} \right)_T \text{grad } E_o^2 - \frac{E_o^2}{2} \left(\frac{\partial \epsilon}{\partial T} \right)_\rho \text{grad } T' \quad (17)$$

$$\text{with } \rho' = -\alpha \rho T', \quad (18)$$

α denoting the coefficient of thermal expansion.

The equation (17) is quite general and can be applied to a fluid dielectric of any shape. Using equation (6), the electric buoyancy force per unit mass for the cylindrical case under consideration can be written as

$$\frac{\vec{f}'}{\rho} = \frac{V_o^2}{\left[\ln \frac{r_2}{r_1} \right]^2} \left[\alpha \left(\frac{\partial \epsilon}{\partial \rho} \right)_T T' \frac{\hat{r}}{r^3} - 1/2 \frac{1}{\rho} \left(\frac{\partial \epsilon}{\partial T} \right)_\rho \cdot \frac{1}{r^2} \text{grad } T' \right] \quad (19)$$

where \hat{r} is the unit radius vector.

Having found an expression for the electric buoyancy force per unit mass, the linearized perturbation equations can be written as follows:

(i) momentum

$$\frac{\partial U_r}{\partial t} = - \frac{\partial}{\partial r} \left(\frac{p'}{\rho_o} \right) + v \left(v^2 U_r - \frac{U_r}{r^2} \right) + \frac{V_o^2}{\left(\ln \frac{r_2}{r_1} \right)^2} \left[\alpha \left(\frac{\partial \epsilon}{\partial \rho} \right)_T \frac{T'}{r^3} - 1/2 \frac{1}{\rho} \left(\frac{\partial \epsilon}{\partial T} \right)_\rho \frac{1}{r^2} \frac{\partial T'}{\partial r} \right] \quad (20)$$

$$\frac{\partial U_{\theta}}{\partial t} = \nu \left[\nabla^2 U_{\theta} - \frac{U_{\theta}}{r^2} \right] \quad (21)$$

$$\frac{\partial U_z}{\partial t} = - \frac{\partial}{\partial z} \left(\frac{p'}{\rho_0} \right) + \nu \nabla^2 U_z - 1/2 \frac{v_0^2}{\left(\ln \frac{r_2}{r_1} \right)^2} \frac{1}{\rho} \left(\frac{\partial \epsilon}{\partial T} \right)_{\rho} \frac{1}{r^2} \frac{\partial T'}{\partial z} \quad (22)$$

(ii) continuity

$$\frac{\partial U_r}{\partial r} + \frac{U_r}{r} + \frac{\partial U_z}{\partial z} = 0 \quad (23)$$

(iii) energy

$$\frac{\partial T'}{\partial t} - \frac{T_1 - T_2}{\ln \frac{r_2}{r_1}} \frac{U_r}{r} = \kappa \nabla^2 T' \quad (24)$$

where ∇^2 has the meaning

$$\nabla^2 = \frac{\partial^2}{\partial r^2} + \frac{1}{r} \frac{\partial}{\partial r} + \frac{\partial^2}{\partial z^2} \quad (25)$$

and ν and κ are the kinematic viscosity and the thermal diffusivity of the fluid.

By analysing the disturbance into normal modes, the solutions of equations (20)-(24) are to be found in the form

$$\left. \begin{aligned} U_r &= e^{pt} U(r) \cos kz, & T' &= e^{pt} \theta(r) \cos kz, \\ U_{\theta} &= e^{pt} V(r) \cos kz, & \frac{p'}{\rho_0} &= e^{pt} \Omega(r) \cos kz, \\ U_z &= e^{pt} W(r) \cos kz. \end{aligned} \right\} (26)$$

where k is the wave number of the disturbance in the axial direction

and p is a constant which may be complex. For solutions of the form (26), equations (20)-(25) reduce to

$$v(DD_* - k^2 - p/v)U + \frac{v_o^2}{(1n \frac{r_2}{r_1})^2} [\alpha (\frac{\partial \epsilon}{\partial \rho})_T \frac{\theta}{r^3} - \frac{1}{2\rho} (\frac{\partial \epsilon}{\partial T})_\rho \frac{1}{r^2} \frac{\partial \theta}{\partial r}] = D\Omega, \quad (27)$$

$$(DD_* - k^2 - p/v)V = 0, \quad (28)$$

$$v(D_*D - k^2 - p/v)W + \frac{1}{2\rho} \frac{v_o^2}{(1n \frac{r_2}{r_1})^2} (\frac{\partial \epsilon}{\partial T})_\rho \frac{k\theta}{r^2} = -k\Omega, \quad (29)$$

$$D_*U = -kW, \quad (30)$$

$$(D_*D - k^2 - p/\kappa)\theta = -\frac{T_1 - T_2}{\kappa \ln \frac{r_2}{r_1}} \frac{U}{r}, \quad (31)$$

$$\text{and } \nabla^2 = D_*D - k^2, \quad (32)$$

$$\text{where } D = \frac{d}{dr} \quad (33)$$

$$\text{and } D_* = \frac{d}{dr} + \frac{1}{r}. \quad (34)$$

For the case when $p=0$ the solution of equation (28) is

$$V = AI_0(kr) + BK_0(kr) \quad (35)$$

where I_0 and K_0 are modified Bessel functions of zeroth order.

Substituting the boundary conditions that on rigid boundaries $V=0$,

we get

$$A = B = 0.$$

$$\text{Hence, } V = 0. \quad (36)$$

This shows that for the form of assumed solutions, there cannot

be any velocity perturbation along θ . Thus, the basic flow is in the form of ring vortices.

Eliminating W between equations (29) and (30), we get

$$-\frac{v_0}{k} (D_*^2 D - k^2 - p/v) D_* U + \frac{1}{2\rho} \frac{v_0^2}{\left(\ln \frac{r_2}{r_1}\right)^2} \left(\frac{\partial \epsilon}{\partial T}\right)_\rho \frac{k\theta}{r^2} = -k\Omega \quad (37)$$

Substituting the above expression for Ω in equation (27), we get after some simplifying steps

$$(DD_* - k^2 - p/v)(DD_* - k^2)U = \frac{v_0^2}{\left(\ln \frac{r_2}{r_1}\right)^2} \frac{k^2}{v} \left[\alpha \left(\frac{\partial \epsilon}{\partial \rho}\right)_T - \frac{1}{\rho} \left(\frac{\partial \epsilon}{\partial T}\right)_\rho\right] \frac{\theta}{r^3} \quad (38)$$

For fluids of uniform composition, the permittivity may be regarded as a function of the state variables alone and we may write

$$\frac{1}{\rho} \left(\frac{\partial \epsilon}{\partial T}\right)_\rho - \alpha \left(\frac{\partial \epsilon}{\partial \rho}\right)_T = \frac{1}{\rho} \left(\frac{\partial \epsilon}{\partial T}\right)_p \quad (39)$$

Thus, equation (38) reduces to

$$(DD_* - k^2 - p/v)(DD_* - k^2)U = -\frac{v_0^2}{\left(\ln \frac{r_2}{r_1}\right)^2} \frac{k^2}{v\rho} \left(\frac{\partial \epsilon}{\partial T}\right)_p \frac{\theta}{r^3} \quad (40)$$

Equation (40) must be solved together with

$$(D_*^2 D - k^2 - p/k)\theta = -\frac{T_1 - T_2}{\kappa \ln \frac{r_2}{r_1}} \cdot \frac{U}{r} \quad (41)$$

Equations (40) and (41) are the marginal stability equations, the solution of which must be found under the boundary conditions

$$U = DU = \theta = 0 \quad (42)$$

at $r=r_1$ and $r=r_2$.

Dimensionless parameters to describe solutions in general form may be obtained by non-dimensionalizing the equations in a suitable manner. A convenient set of non-dimensional variables is

$$\left. \begin{aligned} \zeta &= \frac{r - r_1}{d} \\ \sigma &= \frac{\rho d^2}{\nu} \\ a &= kd \\ \lambda &= \frac{d}{r_1} \end{aligned} \right\} \quad (43)$$

where the cavity gap $r_2 - r_1$ is written as d . The equations (40) through (42) become

$$(D D_* - a^2 - \sigma)(D D_* - a^2)U = - \frac{v_o^2}{\left[\ln \frac{r_2}{r_1}\right]^2} \frac{a^2 d^2}{r_1^3} \frac{1}{\nu \rho} \left(\frac{\partial \varepsilon}{\partial T}\right)_p \frac{\theta}{(1 + \lambda \zeta)^3}, \quad (44)$$

$$(D_* D - a^2 - P\sigma)\theta = - \frac{T_1 - T_2}{\kappa \ln \frac{r_2}{r_1}} \frac{d^2}{r_1} \frac{U}{(1 + \lambda \zeta)}, \quad (45)$$

$$U = DU = \theta = 0 \quad \text{at } \zeta = 0 \text{ and } 1. \quad (46)$$

D and D_* now have the following meaning

$$D = \frac{d}{d\zeta}, \quad (47)$$

$$D_* = \frac{d}{d\zeta} + \frac{\lambda}{1 + \lambda \zeta}, \quad (48)$$

and $P (= \frac{\nu}{\kappa})$ is the Prandtl number.

It is convenient to make the transformation

$$-\frac{\kappa r_1}{(T_1 - T_2)d^2} \ln \frac{r_2}{r_1} \theta \rightarrow \theta, \quad (49)$$

where θ now has the dimensions of velocity.

The marginal stability equations become

$$(DD_* - a^2 - \sigma)(DD_* - a^2)U = -Ra^2 \frac{\theta}{(1 + \lambda\zeta)^3} \quad (50)$$

$$\text{and } (D_*D - a^2 - P\sigma)\theta = \frac{U}{1 + \lambda\zeta} \quad (51)$$

R may be interpreted as the electrical Rayleigh number

$$R = \frac{\alpha g_e \beta d^4}{\nu \kappa} \quad (52)$$

where

$$g_e = -\frac{v_o^2}{r_1^3 \left(\ln \frac{r_2}{r_1}\right)^2} \frac{1}{\rho \alpha} \left(\frac{\partial \epsilon}{\partial T}\right)_p \quad (53)$$

can be regarded as an electrically derived gravity at the surface of the inner cylinder and

$$\beta = \frac{T_1 - T_2}{r_1 \ln \frac{r_2}{r_1}} \quad (54)$$

is the temperature gradient at the inner cylinder surface.

Clearly, the electrical gravity, g_e , is a strong function of radius and varies inversely as the cube of radius.

Table 1

The electrical body force at the inner and outer cylinders.
for a given voltage across the gap.

$$r_1 = 1.711 \times 10^{-2} \text{ m} \qquad \epsilon_0 = 8.854 \times 10^{-12} \text{ farads/m}$$

$$r_2 = 1.903 \times 10^{-2} \text{ m} \qquad \rho = 937.7 \text{ kg/m}^3$$

$$\alpha = 1.08 \times 10^{-3} \text{ cc/cc/}^\circ\text{c} \qquad \frac{\partial}{\partial T} \left(\frac{\epsilon}{\epsilon_0} \right) = 3.72 \times 10^{-3} / ^\circ\text{c}$$

VOLTAGE ACROSS CYLINDERS kv(rms)	($\frac{\text{Electrical gravity}}{\text{Earth's gravity}}$) at $r=r_1$	($\frac{\text{Electrical gravity}}{\text{Earth's gravity}}$) at $r=r_2$
2	0.2343	0.1703
4	0.9372	0.6812
6	2.1087	1.5327
8	3.7488	2.7248
10	5.8575	4.2574
12	8.4348	6.1307

In Table 1, the values of electrical gravity compared to earth's gravity are shown both at the surface of the inner cylinder and that of outer cylinder. At 8.0 kv rms voltage difference between the cylinders, the average electric gravity is three times that of the earth's gravity. Above this voltage difference, it rises even more sharply.

The form of the equations (50) and (51) and the boundary conditions (46) shows that, in the marginal state (i.e. when $\sigma=0$), for a given value

of a , the dimensionless parameters whose values are sufficient to determine uniquely the distribution of U and θ are the electrical Rayleigh number R and the gap to inner radius ratio λ .

2.3 The Exchange of Stabilities

In general σ is a complex quantity and is a function of the physical quantities involved and of the parameters characterizing the particular pattern of the disturbance. If $\text{Re}(\sigma)$ is positive, the disturbance increases, but if it is negative, the disturbance dies away. In a set of possible disturbances, the mode for which $\text{Re}(\sigma)$ is a maximum will be the first to appear beyond stability. When the $\text{Re}(\sigma)$ is just equal to zero, the limiting condition of stability will be realized. It is important to know if the $\text{Im}(\sigma)$ is zero when the $\text{Re}(\sigma)$ is. If $\text{Im}(\sigma)$ is not zero, the disturbance manifests itself in the form of a wave motion and the system is said to be overstable. When $\text{Im}(\sigma)$ is zero if the $\text{Re}(\sigma)$ is zero, we say that the principle of exchange of stabilities is valid. Since the vanishing of σ means that all time variations disappear, this limiting condition represents a steady state in which the disturbance just maintains itself.

To consider the principle of exchange of stabilities for the problem in hand, it is slightly more convenient to write the non-dimensionalized form of equations (40)-(42) with respect to

r_2 , the radius of the outer cylinder. Then, we have

$$(DD_* - a_1^2 - \sigma_1)(DD_* - a_1^2)U = -R_1 a_1^2 \frac{\theta}{r^3} \quad (55)$$

$$(D_* D - a_1^2 - P\sigma_1)\theta = \frac{U}{r} \quad (56)$$

$$\text{and } U = DU = \theta = 0 \text{ at } r = \eta \text{ and } 1. \quad (57)$$

$$\text{where } D = \frac{d}{dr}, \quad D_* = \frac{d}{dr} + \frac{1}{r}, \quad (58)$$

$$a_1 = kr_2 = \frac{ar_2}{d}, \quad (59)$$

$$\sigma_1 = r_2^2 \frac{p}{v} = r_2^2 \frac{\sigma}{d^2}, \quad (60)$$

$$R_1 = \frac{R}{\lambda^4} \quad \text{and} \quad \eta = \frac{r_1}{r_2}. \quad (61)$$

Multiplying equation (55) by rU^* (the star superscripts represent complex conjugates) and integrating in the interval $r = \eta$ and $r = 1$, we get

$$\int_{\eta}^1 rU^*(DD_* - a_1^2 - \sigma_1)(DD_* - a_1^2)U \, dr = -R_1 a_1^2 \int_{\eta}^1 \frac{\theta}{r^2} U^* \, dr \quad (62)$$

Since U and its derivative vanish at the boundaries, the left hand side of equation (62) can be shown to be positive definite (Chandrasekhar, 1961, p297). Thus

$$\begin{aligned} & \int_{\eta}^1 rU^*(DD_* - a_1^2 - \sigma_1)(DD_* - a_1^2)U \, dr \\ &= \int_{\eta}^1 r |(DD_* - a_1^2)U|^2 \, dr + \sigma_1 \int_{\eta}^1 [r \left| \frac{dU}{dr} \right|^2 + \left(\frac{1}{r} + a_1^2 r \right) |U|^2] \, dr \end{aligned} \quad (63)$$

Substituting for U^* from equation (56) in the right hand side of equation (62), we get

$$\int_{\eta}^1 \frac{\theta}{r^2} U^* dr = \int_{\eta}^1 \frac{\theta}{r} (D_* D - a_1^2 - P\sigma^*) \theta^* dr \quad (64)$$

$$= \int_{\eta}^1 \frac{\theta}{r} D_* D \theta^* dr - (a_1^2 + P\sigma^*) \int_{\eta}^1 \frac{|\theta|^2}{r} dr \quad (65)$$

Again making use of the boundary conditions on θ and integrating by parts, we can easily show that

$$\int_{\eta}^1 \frac{\theta}{r} D_* D \theta^* dr = - \int_{\eta}^1 \frac{1}{r} |D\theta|^2 dr + \int_{\eta}^1 \frac{2}{r^2} \theta D\theta^* dr \quad (66)$$

Combining equations (62), (63), (65) and (66), we get

$$\sigma I_1 + I_2 = R_1 a_1^2 [(a_1^2 + P\sigma^*) I_3 + I_4 + I_5] \quad (67)$$

where

$$I_1 = \int_{\eta}^1 [r |DU|^2 + (\frac{1}{r} + a^2 r) |U|^2] dr \quad (68)$$

$$I_2 = \int_{\eta}^1 r | (DD_* - a^2) U|^2 dr \quad (69)$$

$$I_3 = \int_{\eta}^1 \frac{1}{r} |\theta|^2 dr \quad (70)$$

$$I_4 = \int_{\eta}^1 \frac{1}{r} |D\theta|^2 dr \quad (71)$$

and

$$I_5 = -2 \int_{\eta}^1 \frac{\theta}{r^2} D\theta^* dr \quad (72)$$

The integrals I_1 , I_2 , I_3 and I_4 are positive definite while I_5 is complex. Equating the imaginary parts of equation (67), we obtain

$$\text{Im}(\sigma) [I_1 + R_1 a_1^2 P I_3] = R_1 a_1^2 \text{Im}(I_5) \quad (73)$$

and no general conclusions regarding the stability of flow can be drawn from this equation. The validity of the exchange of stabilities cannot be rigorously proved for this problem.

In the next section, it is shown that, for a narrow gap, the stability equations reduce to the form of the Rayleigh-Bénard case. The principle of the exchange of stabilities for the Rayleigh-Bénard form of equations has been proved elsewhere (Chandrasekhar, chapter II). In chapter III, the experiments on electric body force induced convection are described and they show that the instability appears to set in as a stationary convective flow. Without attempting a theoretical justification of the principle of exchange of stabilities, we shall assume its validity to obtain the numerical solution of the eigen-value problem.

2.4 The equations for the case of a narrow gap.

If the gap $r_2 - r_1 (=d)$ between the cylinders is small compared to their mean radius $\frac{r_1 + r_2}{2} (=r_0)$, D_* can be simply replaced by D , (Chandrasekhar, 1961, p 402). In this scheme of approximation, equations (40) and (41) become

$$(D^2 - a^2 - \sigma)(D^2 - a^2)U = - \frac{v_0^2}{\left[\ln \frac{r_2}{r_1}\right]^2} \frac{a^2 d^2}{\nu \rho} \left(\frac{\partial \epsilon}{\partial T}\right)_p \frac{\theta}{r_0^3} \quad (74)$$

$$\text{and } (D^2 - a^2 - P\sigma)\theta = - \frac{(T_1 - T_2)d^2}{\kappa \ln \frac{r_2}{r_1}} \frac{U}{r_0} \quad (75)$$

$$\text{where } \zeta = \frac{r - r_1}{d}, \quad k = \frac{a}{d}, \quad p/\nu = \frac{\sigma}{d^2} \quad (76)$$

The boundary conditions (42) are

$$U \equiv DU \equiv \theta \equiv 0 \text{ at } \zeta=0 \text{ and } 1 \quad (77)$$

By making the transformation

$$- \frac{(T_1 - T_2)d^2}{\kappa \ln \frac{r_2}{r_1}} U \rightarrow U \quad (78)$$

equations (74) and (75) become

$$(D^2 - a^2 - \sigma)(D^2 - a^2)U = -R\theta \quad (79)$$

$$(D^2 - a^2 - P\sigma)\theta = U \quad (80)$$

where

$$R = \frac{\alpha g_e \beta d^4}{\nu \kappa} \quad (81)$$

g_e and β are now defined at the mean radius r_o and have the following meaning

$$g_e = - \frac{V_o^2}{r_o^3 \left(\ln \frac{r_2}{r_1} \right)^2} \frac{1}{\rho \alpha} \left(\frac{\partial \varepsilon}{\partial T} \right)_p \quad (82)$$

and

$$\beta = \frac{T_1 - T_2}{r_o \ln \frac{r_2}{r_1}} \quad (83)$$

Equations (79) and (80) are the same as for Rayleigh-Bénard instability (Chandrasekhar, chapter 2). The principle of exchange of stabilities for this case holds and the instability occurs at a Rayleigh number 1707.762 corresponding to $a = 3.117$.

This analysis serves to show that the principle of exchange of stabilities is valid in the small gap approximation. However, it ignores the curvature effect of the cylinders and cannot be used for any comparison with the experimental results.

2.5 The solution for a wide gap when the marginal state is stationary.

In the marginal state ($\sigma=0$), the equations (55) and (56)

become

$$(DD_* - a_1^2)^2 U = -R_1 a_1^2 \frac{\theta}{r^3} \quad (84)$$

and

$$(D_* D - a_1^2) \theta = \frac{U}{r} \quad (85)$$

On eliminating U between equations (84) and (85), we obtain

$$\begin{aligned} \theta^{VI} + \frac{7}{r} \theta^V + \left(\frac{5}{r^2} - 3a_1^2 \right) \theta^{IV} - \left(\frac{6}{r^3} + \frac{14a_1^2}{r} \right) \theta^{III} \\ + \left(\frac{3}{r^4} - \frac{5a_1^2}{r^2} + 3a_1^4 \right) \theta^{II} - \left(\frac{3}{r^5} - \frac{5a_1^2}{r^3} - \frac{7a_1^4}{r} \right) \theta^I \\ - a_1^6 \theta = -R_1 a_1^2 \frac{\theta}{r^4} \end{aligned} \quad (86)$$

with the appropriate boundary conditions

$$\theta = \theta^{II} + \frac{1}{r} \theta^I - a_1^2 \theta = \theta^{III} + \frac{2}{r} \theta^{II} - a_1^2 \theta^I - \frac{a_1^2}{r} \theta = 0 \quad (87)$$

at $r = \frac{r_1}{r_2}$ and 1.

Alternately, we can eliminate θ between equations (84) and (85).

The eigenvalue problem, then, becomes

$$\begin{aligned} U^{VI} + \frac{9}{r} U^V + \left(\frac{16}{r^2} - 3a_1^2 \right) U^{IV} + \left(\frac{2}{r^3} - \frac{18a_1^2}{r} \right) U^{III} - \left(\frac{3}{r^4} + \frac{23a_1^2}{r^2} - 3a_1^4 \right) U^{II} \\ + \left(\frac{3}{r^5} - \frac{5a_1^2}{r^3} + \frac{9a_1^4}{r} \right) U^I - \left(\frac{3}{r^6} - \frac{5a_1^2}{r^4} - \frac{7a_1^2}{r^2} + a_1^6 \right) U = -R_1 a_1^2 \frac{U}{r} \end{aligned} \quad (88)$$

subject to boundary conditions

$$U \equiv U^I \equiv U^{IV} + \frac{2}{r} U^{III} - \left(\frac{3}{r^2} + 2a_1^2 \right) U^{II} + \left(\frac{3}{r^3} - \frac{2a_1^2}{r} \right) U^I - \left(\frac{3}{r^4} - \frac{2a_1^2}{r^2} - a_1^4 \right) U \equiv 0$$

at $r = \frac{r_1}{r_2}$ and 1. (89)

The critical values of R_1 and a_1 were found by solving numerically equation (86) with boundary conditions (87).

The general solution of equation (86) is

$\theta = A_1 \theta_1 + A_2 \theta_2 + A_3 \theta_3 + A_4 \theta_4 + A_5 \theta_5 + A_6 \theta_6$, where A_1, A_2, \dots, A_6 are constants. The condition that these solutions $\theta_1, \theta_2, \dots, \theta_6$ form a fundamental set is that their Wronskian is not zero. There is an

infinite number of possible sets of solutions. One simple set can be found by choosing $\theta_1(r)$ such that

$$\theta_1(r_1/r_2) = 1, \theta_1^I(r_1/r_2) = \theta_1^{II}(r_1/r_2) = \dots = \theta_1^V(r_1/r_2) = 0 \quad (90)$$

and defining $\theta_n(r)$ where $n = 2, 3, \dots, 6$ as that solution which satisfies the initial conditions

$$\theta_n^{m-1}(r) = 0 \quad \text{if } m \neq n, m = 1, 2, \dots, 6 \quad (91)$$

$$\theta_n^{m-1}(r) = 1 \quad \text{if } m = n, m = 1, 2, \dots, 6 \quad (92)$$

Then $\theta_1(r), \theta_2(r), \dots, \theta_6(r)$ form a fundamental set and the value of their Wronskian at $r = \frac{r_1}{r_2}$ is unity (Ince, 1956, p 119).

For a given value of a_1 and R_1 the solutions $\theta_1(r), \theta_2(r), \dots, \theta_6(r)$, with the initial conditions (90)-(92), were found numerically by the method of Runge-Kutta by breaking the sixth order differential equation (86) into six simultaneous first order equations (Ford, 1955, chapter 6) by writing

$$\theta^I = G$$

$$\theta^{II} = H$$

$$\theta^{III} = J$$

$$\theta^{IV} = K$$

$$\theta^V = L$$

and

$$\begin{aligned} & L^I + \frac{7}{r} L + \left(\frac{5}{r^2} - 3a_1^2\right)K - \left(\frac{6}{r^3} + \frac{14a_1^2}{r}\right)J + \left(\frac{3}{r^4} - \frac{5a_1^2}{r^2} + 3a_1^4\right)H \\ & - \left(\frac{3}{r^5} - \frac{5a_1^2}{r^3} - \frac{7a_1^4}{r}\right)G + \left(R_1 \frac{a_1^2}{r^4} + a_1^6\right)\theta = 0 \end{aligned} \quad (93)$$

Knowing $\theta_1(r)$, $\theta_2(r)$... $\theta_6(r)$ and thus θ , the boundary conditions (87) were substituted to give a set of six linear homogeneous equations (three at the inner boundary and three at the outer boundary). The condition that they have a non-trivial solution is that the determinant

$$\text{DET} = \begin{vmatrix} a_{11} & a_{12} & a_{13} & a_{14} & a_{15} & a_{16} \\ a_{21} & & & & & \\ a_{31} & & & & & \\ a_{41} & & & & & \\ a_{51} & & & & & \\ a_{61} & a_{62} & a_{63} & \dots\dots\dots & a_{66} & \end{vmatrix} = f(a_1, R_1) = 0 \quad (94)$$

where a_{1j} ($j = 1 \dots 6$) are the coefficients of A_j in the first equation; a_{2j} are coefficients of A_j in the second equation and so on.

For a given value of a_1 , some value of R_1 will cause the determinant to vanish. To find that value, determinant (94) was calculated for increasing values of R_1 till the determinant changed sign. Knowing positive and negative values of the determinant corresponding to two values of R_1 , a linear interpolation scheme (regula falsi method, Mathews and Walker, 1964, p339) was used

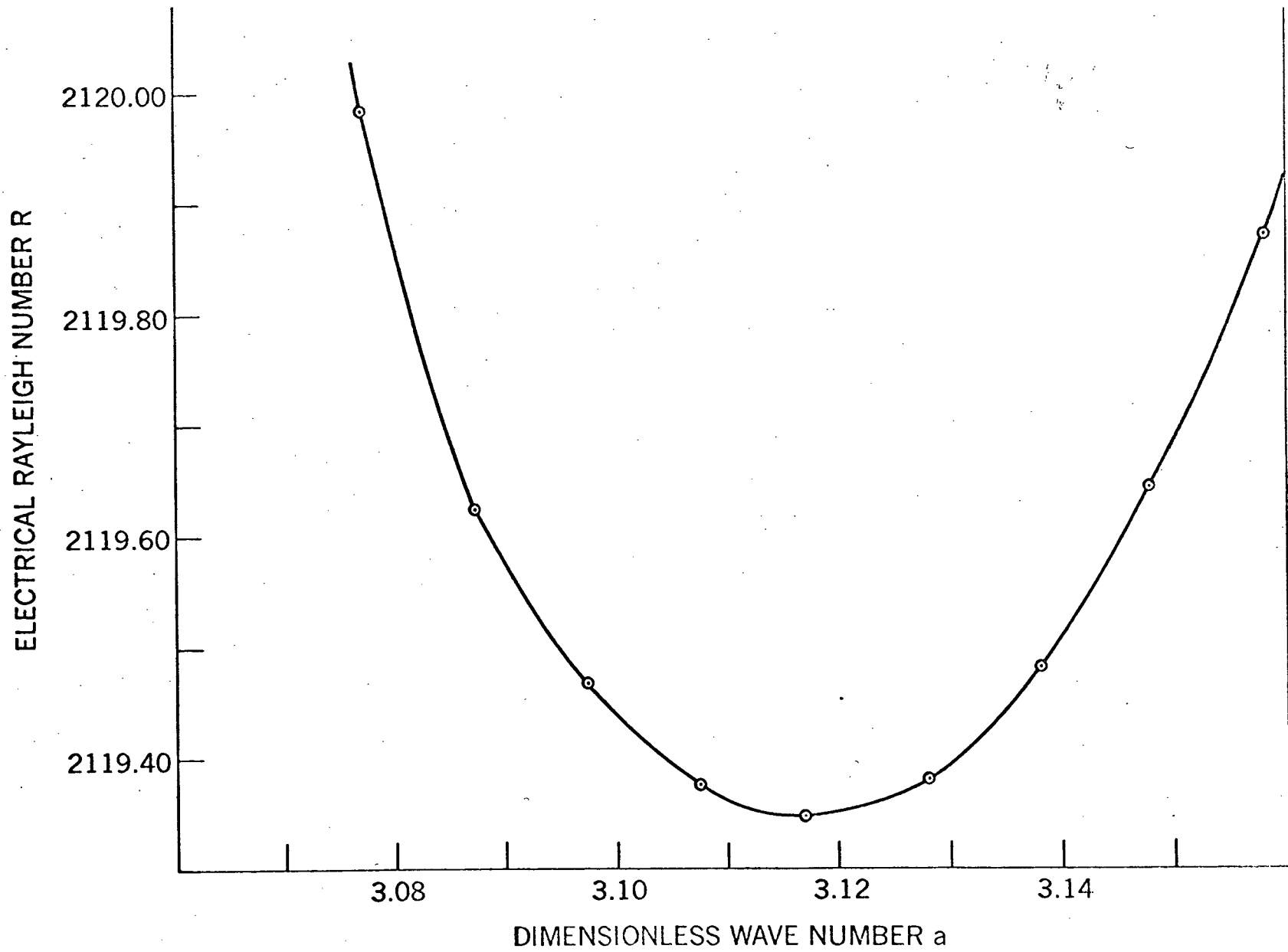


FIGURE 2. DEPENDENCE OF THE NUMERICALLY DETERMINED ELECTRICAL RAYLEIGH NUMBER ON THE DIMENSIONLESS WAVE NUMBER.

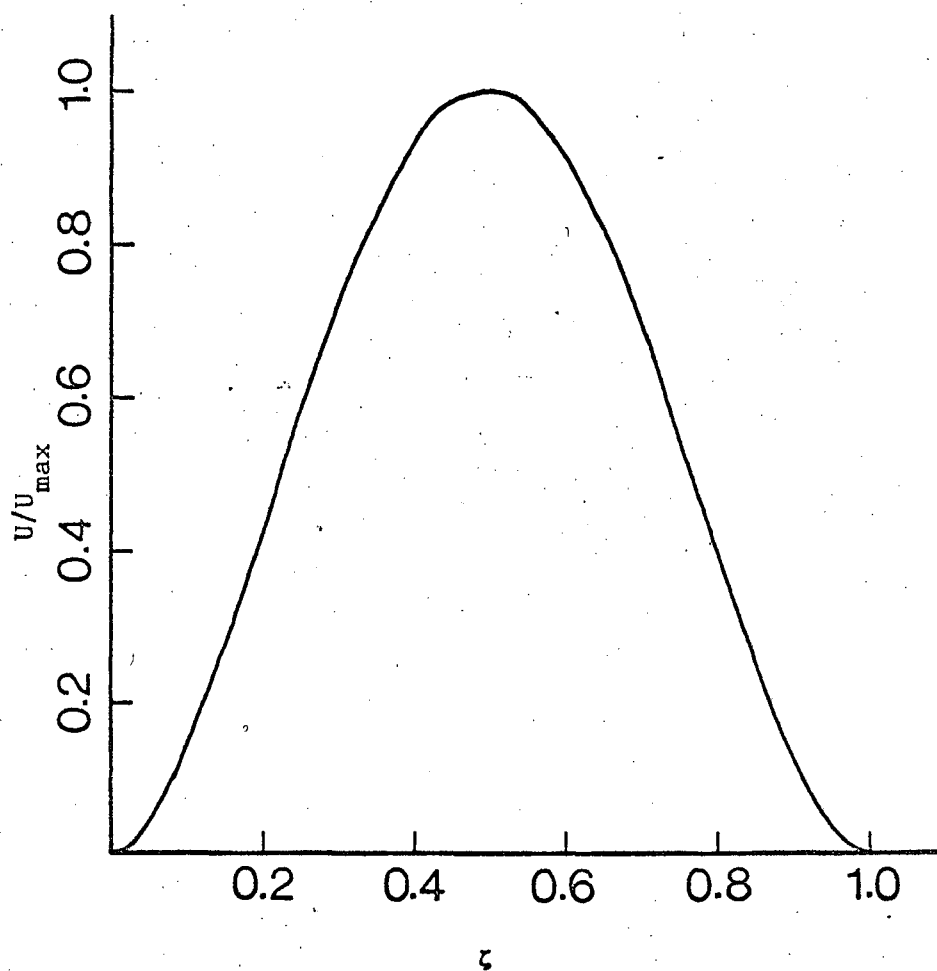


FIGURE 3. THE VELOCITY PROFILE AT THE ONSET OF CONVECTION. THE VELOCITY IS NORMALIZED TO UNIT MAXIMUM AMPLITUDE.

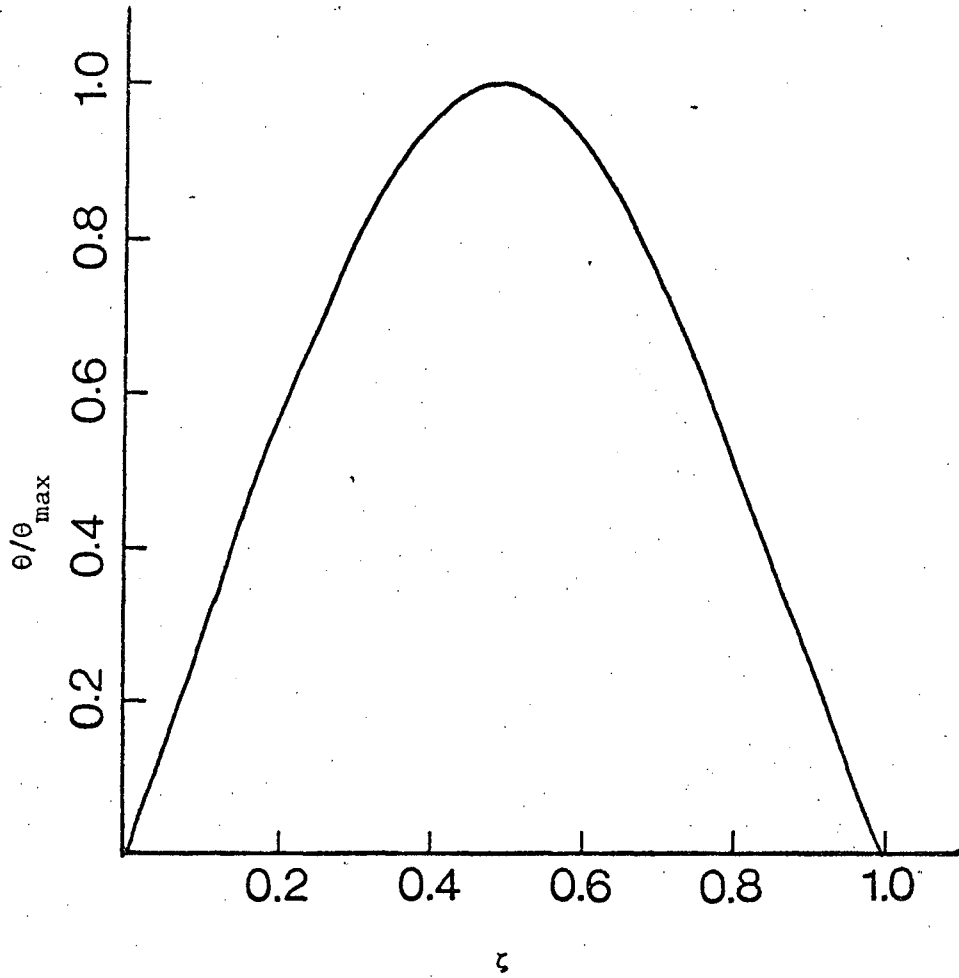


FIGURE 4. THE TEMPERATURE PROFILE AT THE ONSET OF CONVECTION. THE TEMPERATURE IS NORMALIZED TO UNIT MAXIMUM AMPLITUDE.

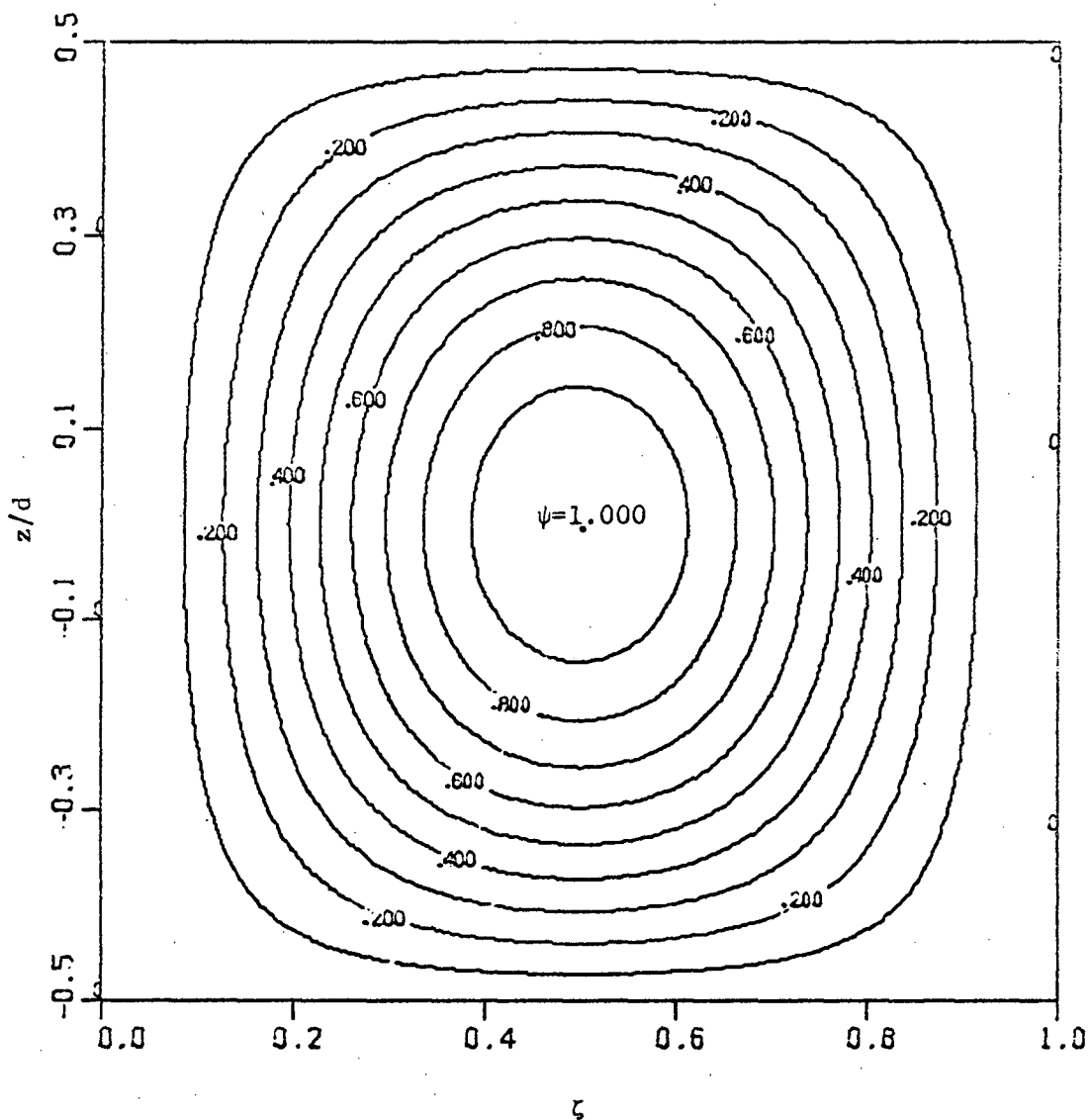


FIGURE 5. THE STREAMLINES AT THE ONSET OF INSTABILITY. THE STREAM FUNCTION ψ (PROPORTIONAL TO $rU \cos az$) HAS BEEN NORMALIZED TO UNITY AND THE CELL PATTERN IS DRAWN SYMMETRICALLY ABOUT $z=0$. THE UNIT OF LENGTH IS THE THICKNESS OF THE ANNULUS.

to iterate and find R_1 for which the determinant vanished. R_1 , in general, converged to a finite value (to eight significant figures) within six iterations. For these values of a_1 and R_1 , the value of the determinant was less than 10^{-12} and was considered adequate. Knowing a_1 and R_1 , the corresponding values of a and R were found by making use of equations (59) and (61). The results of these computations are shown in figure 2.

The solution of interest is the minimum value of R for which $f(a,R) = 0$. Quadratic iteration was used here to find the value of a for which R is minimum. The method has been described by McFadden(1969). The critical values of R_c and a_c found numerically are

$$R_c = 2119.346.; \quad a_c = 3.117$$

using the values

$$r_1 = 1.711 \text{ cms.}; \quad r_2 = 1.903 \text{ cms.}$$

for the radii of the cylinders.

These values were also calculated by solving the sixth-order equation in U and were found to agree within three decimal places (seven significant figures).

Figure 3 shows the profile of the velocity distribution corresponding to R_c and a_c . Figure 4 shows the temperature distribution. The stream lines at the onset of instability are shown in figure 5.

CHAPTER III

EXPERIMENTAL ARRANGEMENT AND RESULTS

3.1 Introduction

Chandra(1969) has described the cylindrical experimental arrangement in detail. He also presented some preliminary results on electrical body force driven convection. Although the heat transfer measurements clearly indicated the change from conduction to convection regime, the measured Nusselt number (ratio of total heat transfer to heat transfer by conduction alone) in the conduction regime was found to be 10-15% less than its value of unity. No definite explanation for this discrepancy could be given. However, it was suspected that the discrepancy arose partly due to the heat losses from the ends of the heating coil and partly due to the errors in the inference of the temperature of the outer cylinder. The outer cylinder was cooled by transformer oil kept at a constant temperature by circulating it through an external thermostatic bath. The temperatures at the inlet and outlet points (figure 6, 11 and 12) to the thermal flask were measured and their mean was taken to be the temperature of the outer cylinder. However, for a short contact time of flowing liquid at a temperature lower than that of the solid wall, the fluid temperature changes appreciably only in the immediate vicinity of the wall (Bird, Stewart and Lightfoot, 1966, p349). Away

from the wall, there is hardly any change in fluid temperature even when there is increased heat transfer between the cylinders.

It was therefore, felt necessary to do the experiments again to be able to compare experimental results with theoretical values. In these experiments, the heating coil was placed much closer to the wall of the inner cylinder to minimize heat loss from the ends and to assure radial heat transfer. However, heat transfer and temperature measurements showed that this could not account for the observed discrepancy.

Next, temperature of the outer cylinder was measured at zero applied potential independent of the inlet and outlet temperatures. The true temperature of the outer cylinder was found to be different from the mean. A linear relation was obtained between the mean of the inlet and outlet temperatures and the true temperature of the outer cylinder. This was done only when there was no potential difference across the cavity. When the outer cylinder was at a high voltage, its temperature could not be measured directly. However, from the linear relationship, the temperature of the outer cylinder was found indirectly under the assumption that the flow and temperature distribution in the thermal flask are not altered by the high voltage. The Nusselt number now gave a value of unity in the conduction regime.

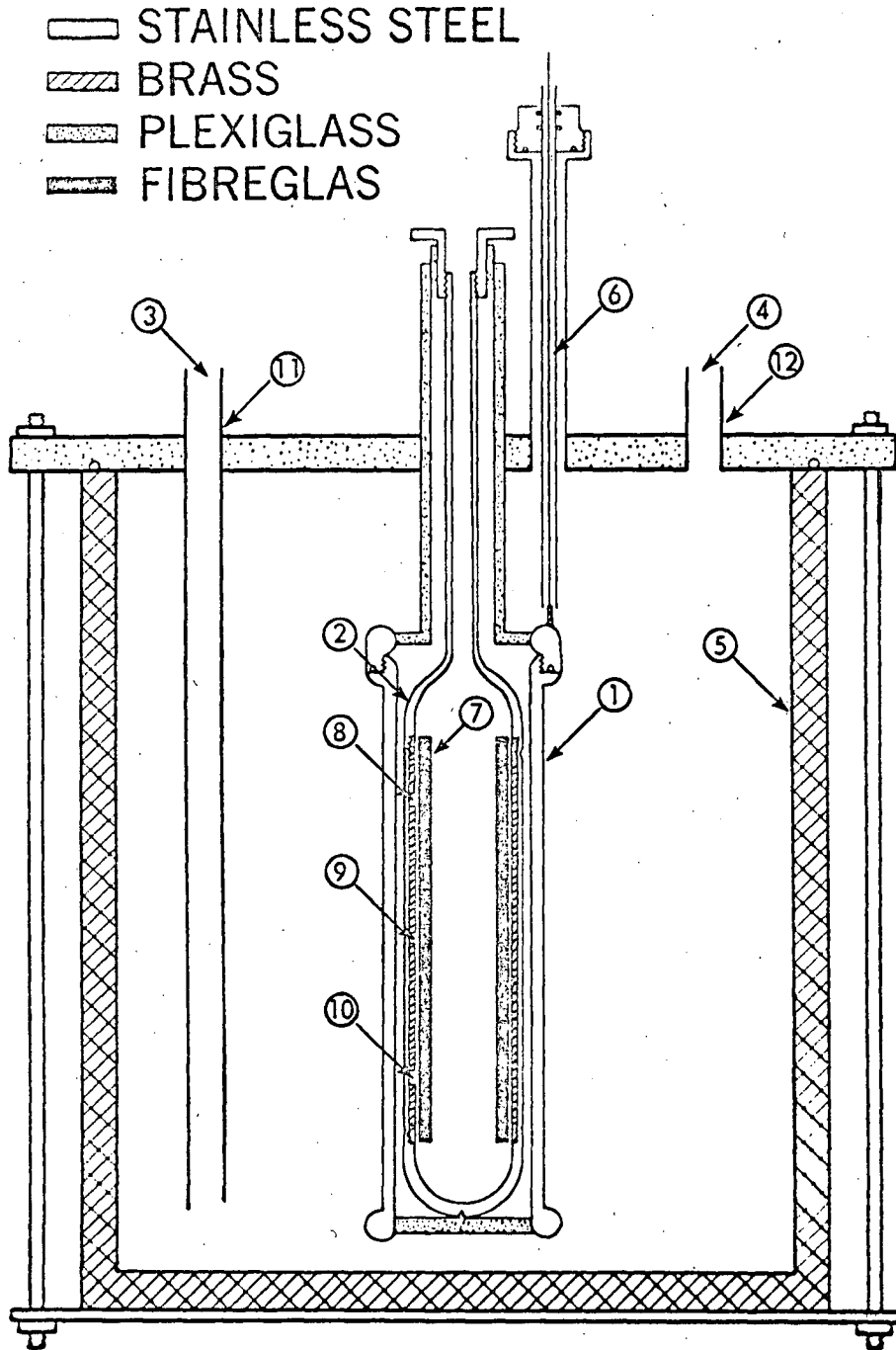


FIGURE 6. A CROSS SECTION OF THE APPARATUS.

3.2 Experimental Arrangement

The apparatus, detailed in figure 6, consisted of two coaxial cylinders (1 and 2) of stainless steel. The cylinders were polished to a mirror finish to avoid any sharp points which might cause electric breakdown at high voltages.

The inner cylinder (2) was constructed in two parts. The central part was made from brass tubing in which holes at 8, 9 and 10 were drilled to accept thermistors. A tight fitting stainless steel tubing was then forced over the brass tubing. End pieces were machined from stainless steel and fitted to the central part with inside corners at the lines of contact to prevent the occurrence of corona. The heating coil (7), made of a close wound 30 S.W.G. diamel coated 'Mancoloy 10' wire on a fibreglass rod, was a close fit inside the inner cylinder. After installing calibrated thermistors in the receptacles at 8, 9 and 10, the heating coil was centered and the remaining space inside the inner cylinder was filled with thermal epoxy and allowed to set. Besides the end points, the heating coil was also tapped at two intermediate points directly opposite the thermistors at 8 and 10. The leads for the thermistors and the heating coil were brought out the top of the cylinders.

The inner cylinder was located coaxially inside the outer cylinder (1) by means of plexiglass centering devices at each end. The locations of the centering devices were well beyond the measurement length between the points 8 and 10. The outer cylinder was equipped with toroidal terminations to prevent the occurrence of

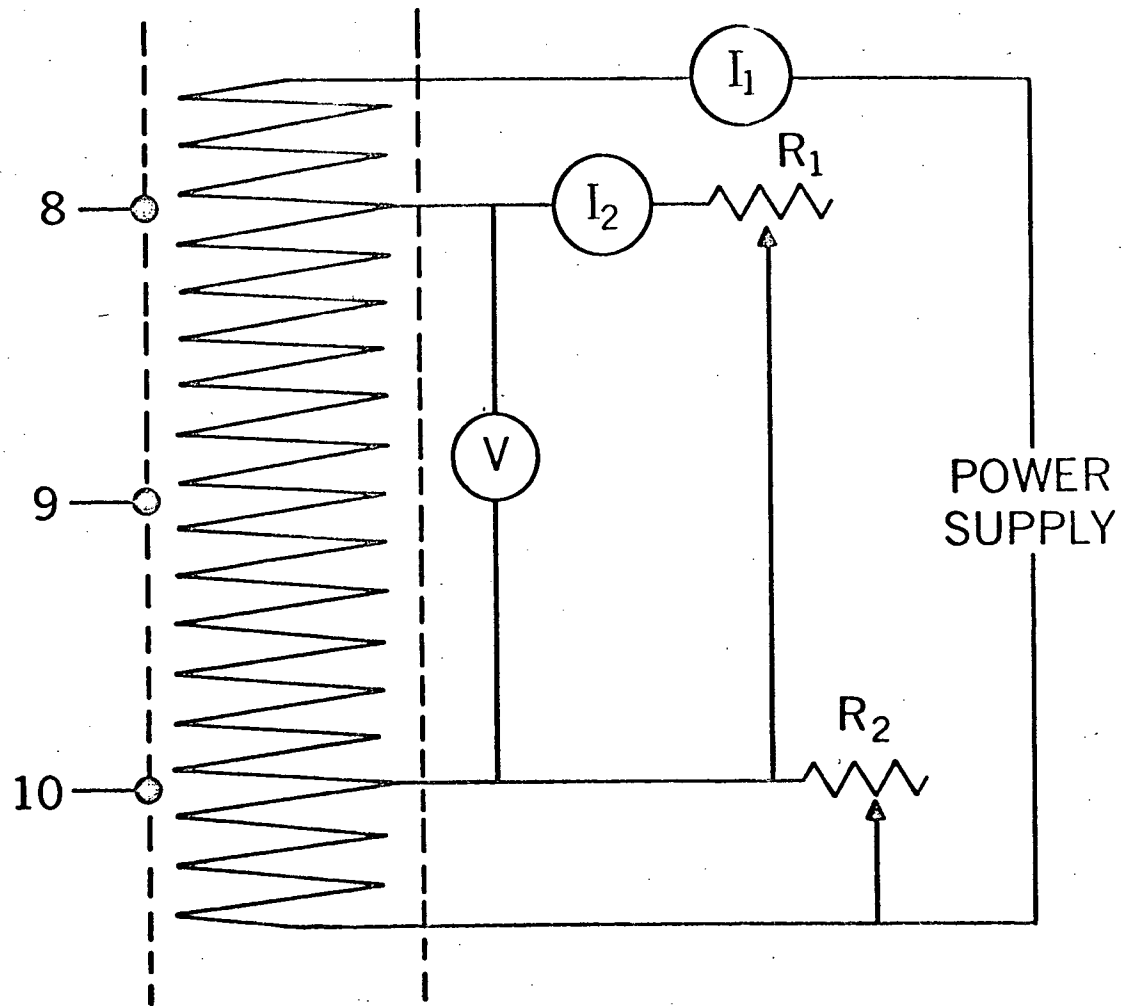


FIGURE 7. THE CIRCUIT FOR THE PLATING COIL.

corona. Table 2 summarizes the important dimensions of the completed cell.

Table 2
Cell Dimensions.

Radius of the inner cylinder

Inner radius = 1.455 ± 0.002 cms.

Outer radius = 1.711 ± 0.002 cms.

Radius of the outer cylinder

Inner radius = 1.903 ± 0.002 cms.

Outer radius = 2.114 ± 0.002 cms.

Length of the measurement section between the points 8 and 10

$L = 8.25 \pm 0.02$ cms.

The assembled apparatus was set in a double walled thermal flask (5) filled with transformer oil. This oil was circulated through an external thermostat, thus enabling the temperature of the outer cylinder to be maintained constant. The temperature in the thermal flask could be controlled to $\pm 0.02^{\circ}\text{C}$.

The present setup did not allow to observe fluid motions visually. The onset of thermal convection was detected by making heat transfer and temperature measurements.

The Heating Circuit: The control circuit for the heating coil is shown in figure 7. As already mentioned, the heater was a three sectioned heating element. Currents in the three sections were adjusted by means of the rheostats R_1 and R_2 until the thermistors at 8, 9 and 10 gave the same temperature reading (control to about 0.01°C was found feasible) to ensure uniformity of temperature

T_1 on the surface of the inner cylinder. At equilibrium the heat transfer occurring in the section between the points 8 and 10 was taken to be equal to the dissipation of electrical energy in the central section of the coil. The ammeters I_1 and I_2 and the voltmeter V_1 were all of 1% accuracy (made by Weston, Model 81). The current for the heating element was drawn from a direct current (Hewlett Packard, model 6290A) power supply. The power input in the central section of the coil is given by

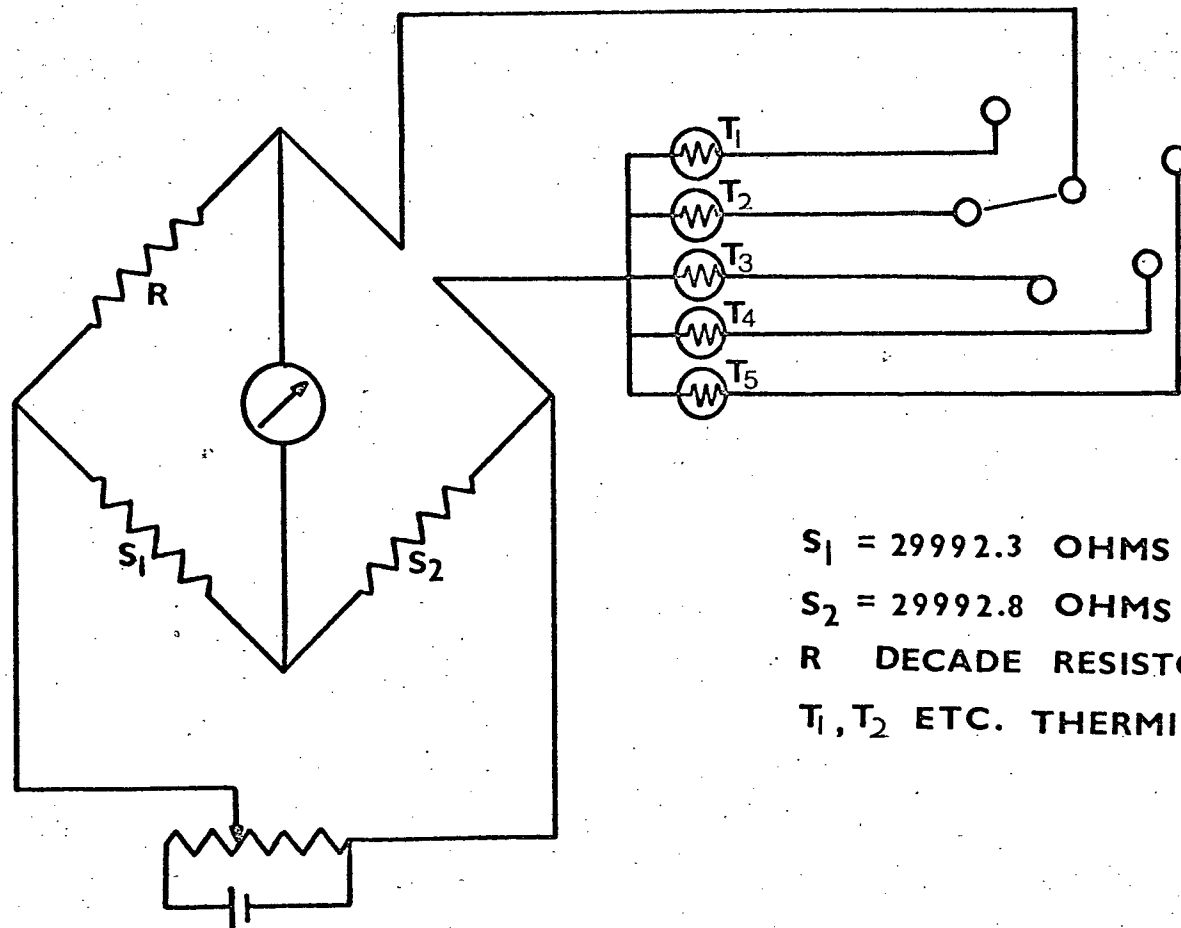
$$(i_1 - i_2) v_1 \text{ watts}$$

The Thermistors: The glass coated thermistors of .043 in. diameter had a nominal resistance of $50,000 \pm 20\%$ ohms at 25°C and a dissipation constant in air of 0.7 milliwatts per $^\circ\text{C}$. All thermistors were calibrated before use. The calibration was performed against a N.P.L. calibrated platinum resistance thermometer. The calibration points were recorded over a $15\text{--}28^\circ\text{C}$ interval. The results were analyzed by the method of least squares for fit to the orthogonal polynomials for the function

$$\ln R = A + B/T + C/T^2$$

where R is the resistance of the thermistor at temperature $T^\circ\text{C}$ and A , B and C are the constants of the cubic equation.

The results of calibration and the difference between the calibration resistance and the computed resistance are listed in tables 3 and 4 (Appendix 1).



$S_1 = 29992.3 \text{ OHMS}$
 $S_2 = 29992.8 \text{ OHMS}$
 R DECADE RESISTOR
 T_1, T_2 ETC. THERMISTORS

FIGURE 8. THE BRIDGE CIRCUIT.

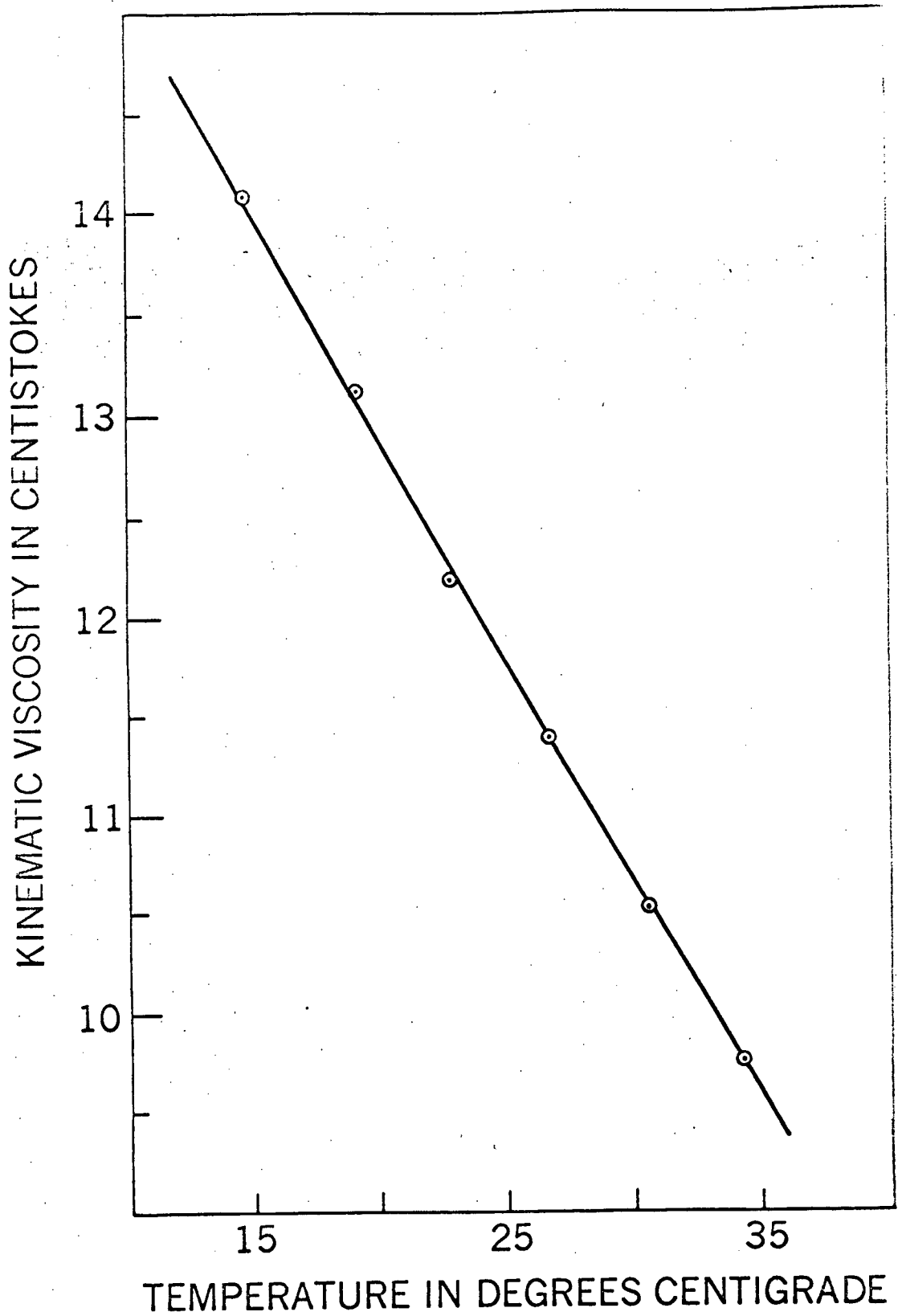


FIGURE 9. KINEMATIC VISCOSITY AS A FUNCTION OF TEMPERATURE.

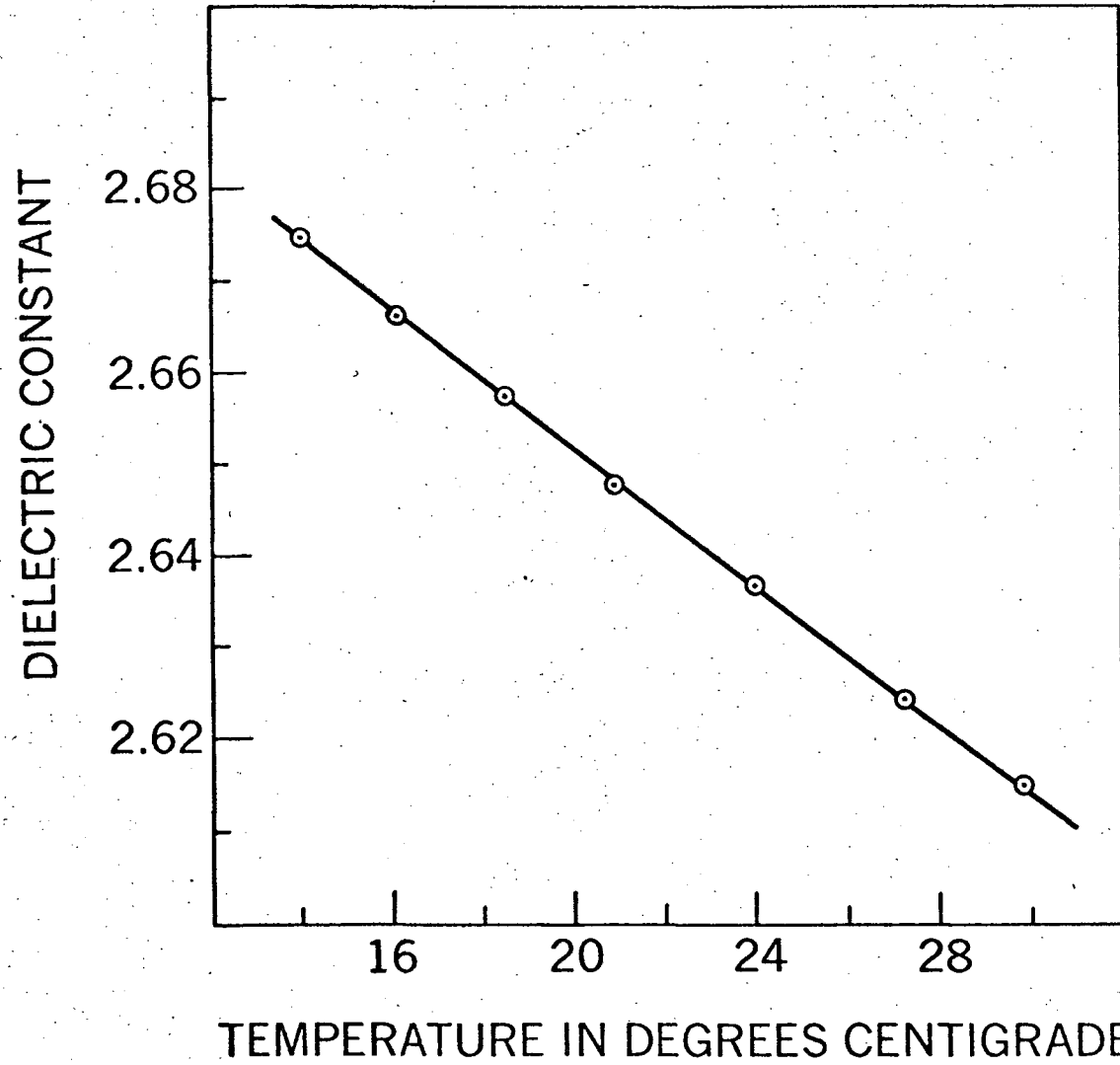


FIGURE 10. DIELECTRIC CONSTANT AS A FUNCTION OF TEMPERATURE.

The resistance of the thermistors was read with a direct reading bridge specially designed for this purpose (figure 8).

The High Voltage Supply: In all experiments, the inner cylinder was grounded and the outer cylinder was kept at a high alternating voltage. The 60 Hz high voltage was supplied from a step-up transformer made by the Universal Voltronics Corporation. A voltage stabilizer was inserted between the mains and the input to the transformer. This eliminated the fluctuations of the power line and gave a constant output voltage.

A high accuracy (1%) electrostatic voltmeter was used to measure the applied potential difference between the cylinders,

The Dielectric Liquid: The dielectric liquid for these experiments was DC200 electrical grade silicone oil (supplied by Dow Corning) whose physical properties are listed in table 5. The silicone oil was selected because it has a high electric strength and is available commercially in any desired viscosity grade. The dynamic viscosity and the dielectric constant of the oil as a function of temperature were measured using a falling ball viscometer and a standard capacitive cell respectively. In figure 9, the kinematic viscosity of the oil is plotted as a function of temperature. Figure 10 shows the variation of dielectric constant with temperature. Other properties listed in table 5 are taken from Dow Corning Bulletin 05-213 of July 1968.

Table 5

Physical Properties of Silicone Oil*

Density, $\rho = 0.9377 \text{ gm. cm}^{-3}$
Coefficient of volume expansion, $\alpha = 1.08 \times 10^{-3} \text{ }^{\circ}\text{C}^{-1}$
Thermal conductivity, $\chi = 3.2 \times 10^{-4} \text{ cal. cm}^{-1} \text{ sec}^{-1} \text{ }^{\circ}\text{C}^{-1}$
Specific heat, $C_p = 0.43 \text{ cal. gm.}^{-1} \text{ }^{\circ}\text{C}^{-1}$
Dielectric constant, $\kappa_e = 2.64$
Kinematic viscosity, $\nu = 12.225 \text{ cm}^2 \text{ sec}^{-1}$

*All properties are given at 23°C.

3.3 Experimental Procedure:

The cylindrical annulus, previously cleaned, was filled with degassed electric grade silicone oil. The cavity was further connected to a vacuum pump to remove any tiny bubbles sticking to the walls of the cylinders. Having made all electrical connections, the external thermostat was switched on. In all experiments, the temperature of the outer cylinder, T_2 , was kept lower than the temperature of the inner cylinder, T_1 .

An initial run, to correlate the temperature of the outer cylinder, T_2 , with the mean of the inlet and outlet temperatures, was done without any high voltage across the cylinders. For this, two thermistors were attached to the wall of the outer cylinder. The inner cylinder was heated and when the conditions became stable, the temperatures at points 8, 9 and 10 (figure 6) were measured. The currents in the three sections of the heating coil were adjusted

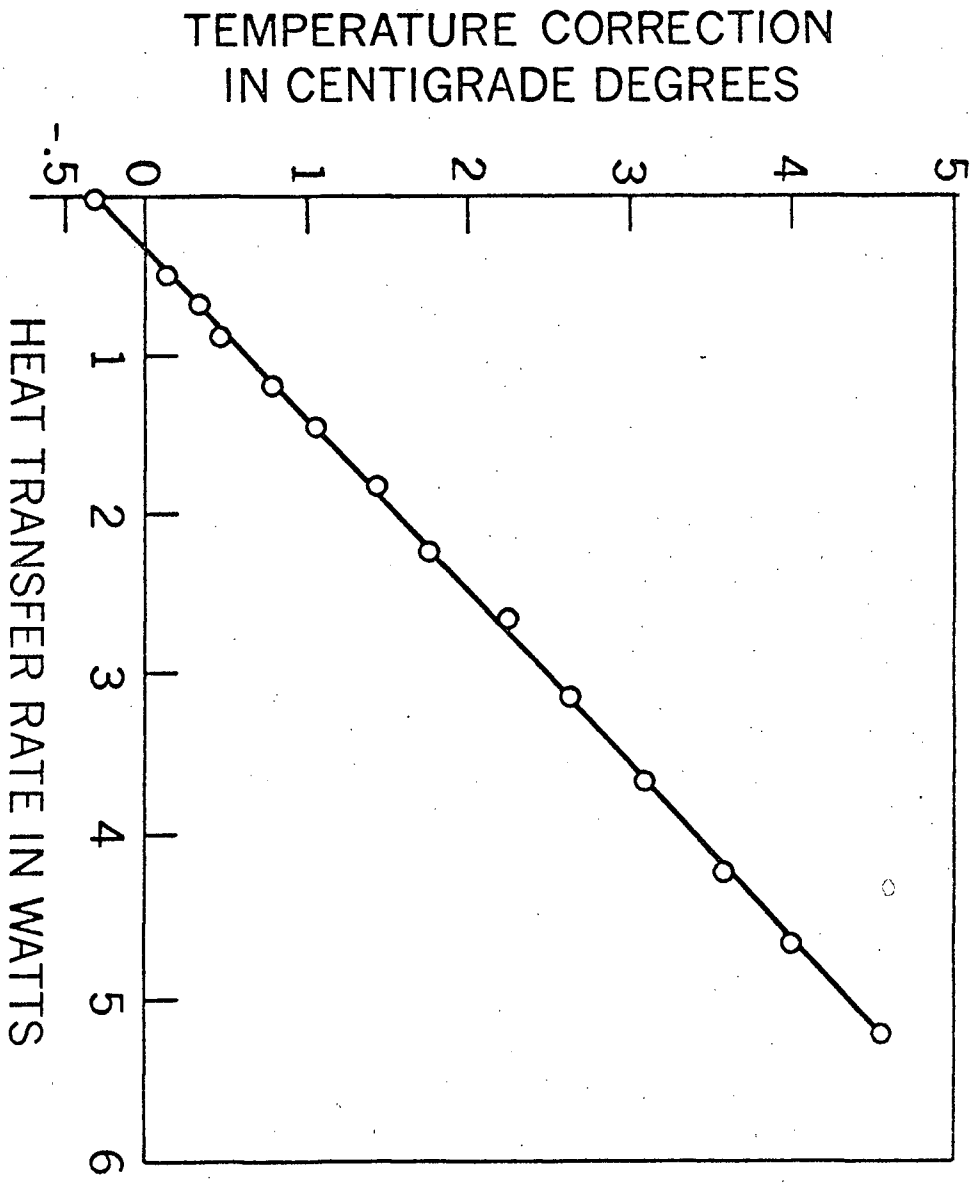


FIGURE 11. DEPENDENCE OF THE TEMPERATURE OF THE OUTER CYLINDER LESS MEAN OF INLET-OUTLET TEMPERATURES ON HEAT TRANSFER RATE.

with rheostats R_1 and R_2 (figure 7) until all the temperature readings on the surface of the inner cylinder were within 0.01°C . The temperature of the outer cylinder and that of the inlet and outlet points were all noted. After 10 minutes, all temperatures were measured again and if there was no change then the readings were accepted. The procedure was repeated for several values of heat transfer rate across the cavity. It was found that the actual temperature of the outer cylinder less the mean temperature read by the inlet and outlet thermistors (11 and 12 in figure 6) is linear in the heat transfer rate between the cylinders as shown in figure 11.

When the heat transfer and temperature measurements were done with the outer cylinder at a high alternating potential, it was not possible to measure its temperature. Since the flow and heat transfer in the circulated transformer oil filling the thermal flask are likely to be largely unaffected by the potential of the outer cylinder, it was assumed that this is precisely so. Knowing the heat transfer rate and the mean of inlet-outlet temperatures, the plot shown in figure 11 provided an indirect means of obtaining the temperature of the outer cylinder.

The experiments were run for the following values of potential difference across the gap.

0 kv rms, 4.06 kv rms, 6.00 kv rms, 6.92 kv rms, 7.91 kv rms, 9.63 kv rms, 10.15 kv rms, 10.80 kv rms.

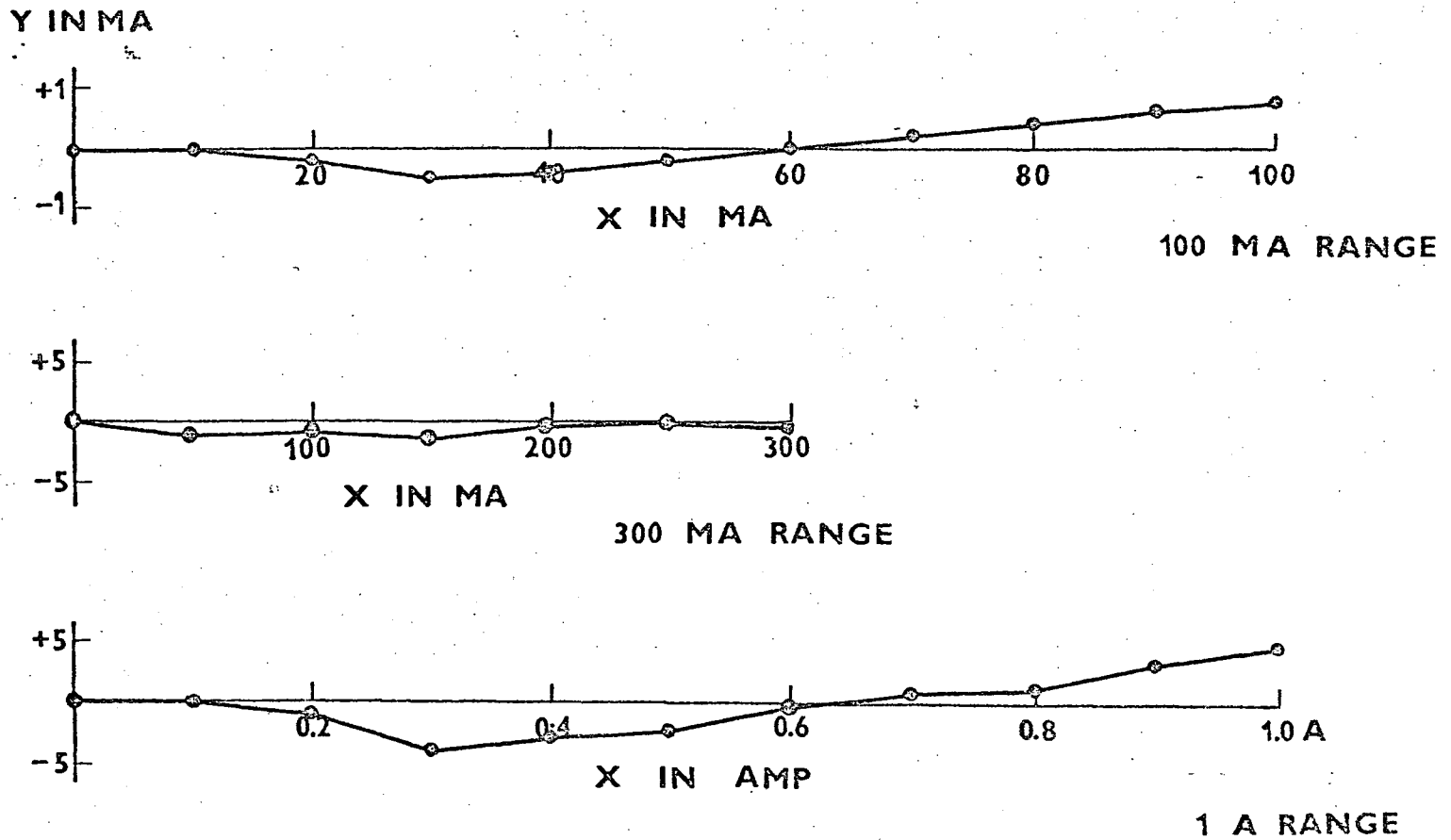


FIGURE 12. DIFFERENCE BETWEEN THE READING OF AMMETER I_1 AND LABORATORY STANDARD AS A FUNCTION OF THE AMMETER READING FOR DIFFERENT CURRENT RANGES. THE CURRENT DIFFERENCE IS PLOTTED AS Y AND THE AMMETER READING AS X.

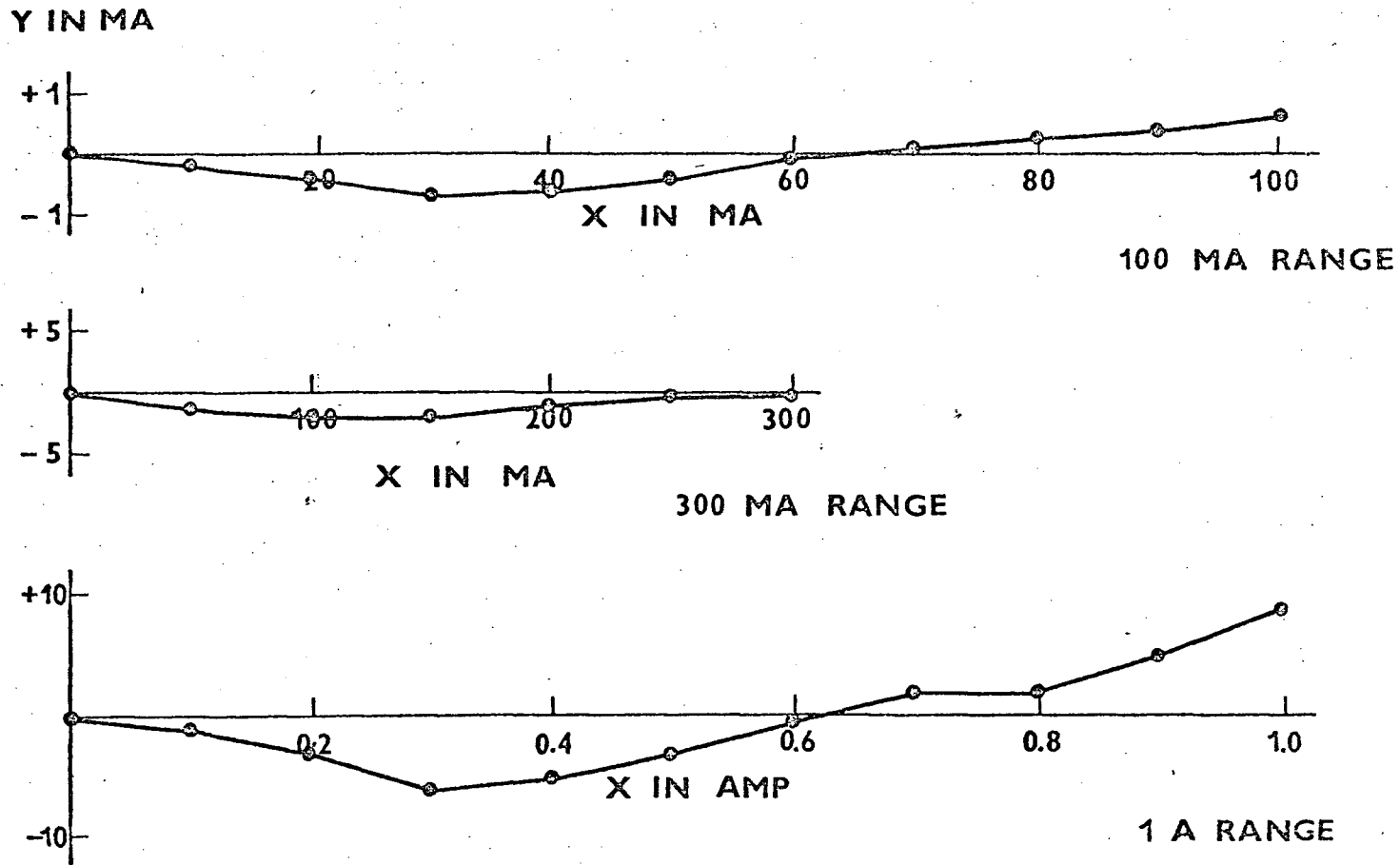


FIGURE 13. DIFFERENCE BETWEEN THE READING OF AMMETER I_2 AND LABORATORY STANDARD AS A FUNCTION OF THE AMMETER READING FOR DIFFERENT CURRENT RANGES. THE CURRENT DIFFERENCE IS PLOTTED AS Y AND THE AMMETER READING AS X.

Y IN VOLTS

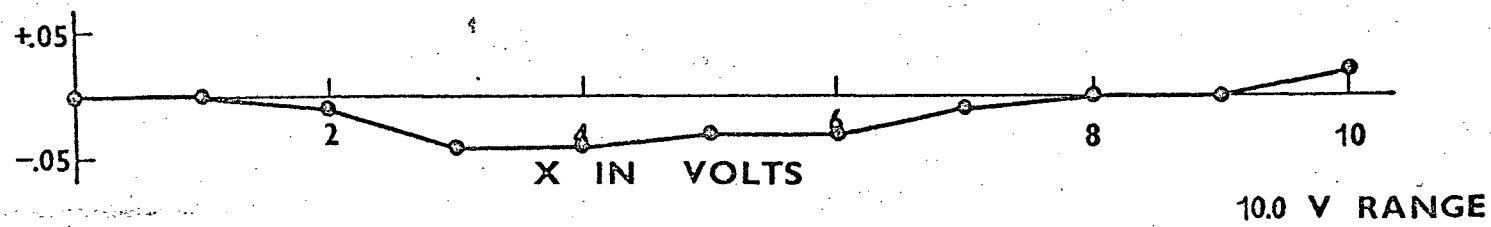
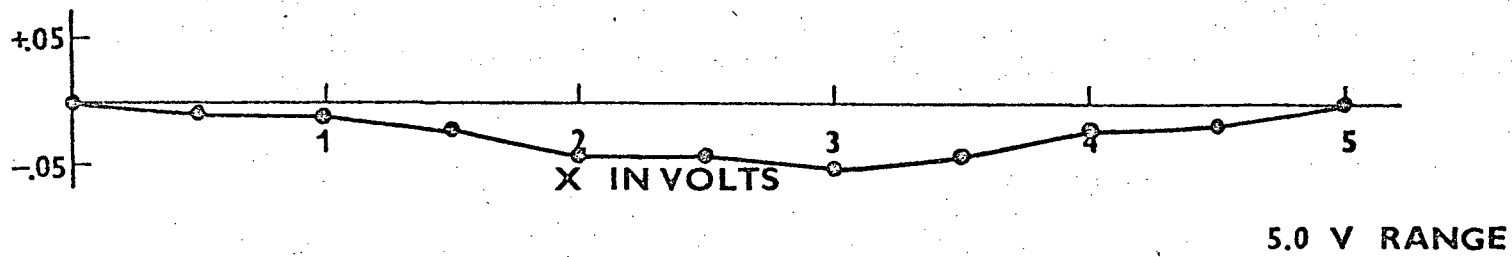
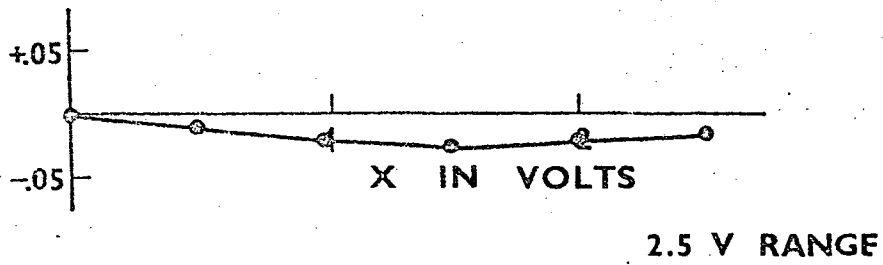


FIGURE 14. DIFFERENCE BETWEEN THE READING OF THE VOLTMETER V_1 AND LABORATORY STANDARD AS A FUNCTION OF THE VOLTMETER READING FOR DIFFERENT VOLTAGE RANGES. THE VOLTAGE DIFFERENCE IS PLOTTED AS Y AND THE VOLTMETER READING AS X.

All the observed data is tabulated in tables 6-13 (Appendix II).

3.4 Errors and corrections.

The ammeters I_1 and I_2 and the voltmeter V_1 (figure 7) were calibrated against a laboratory standard of 0.1% accuracy. The results of calibration are shown in figures 12-14. All values of currents and voltages were reduced using these graphs. The corrected values of i_1 , i_2 and v_1 and the average temperatures of the inner and outer cylinders are tabulated in tables 14 through 21 (Appendix III).

Errors due to self heating of the thermistors: The thermistors were specified to have a dissipation constant in air of 0.7 milliwatt per °C. Accordingly, a power of 0.7 milliwatt in the thermistor will change its temperature by 1°C which will in turn change its resistance by about 5%. This is referred to as a self-heating error. It can be reduced by properly selecting the bridge voltage.

The self-heat effect was restricted to less than the 0.01°C allowable precision. Taking a reasonable amount of error due to self-heating to be 50% of allowable precision or 0.005°C, the maximum power allowed through the thermistor is $0.7 \times 0.005 = 3.5 \times 10^{-6}$ watts.

Taking an average value for the resistance of the thermistor to be 50,000Ω, we get for the voltage across the thermistor a value $3.5 \times 10^{-6} \times 50 \times 10^3$ or 0.42 volts. We can, therefore, use a maximum of 0.84 volts across the bridge.

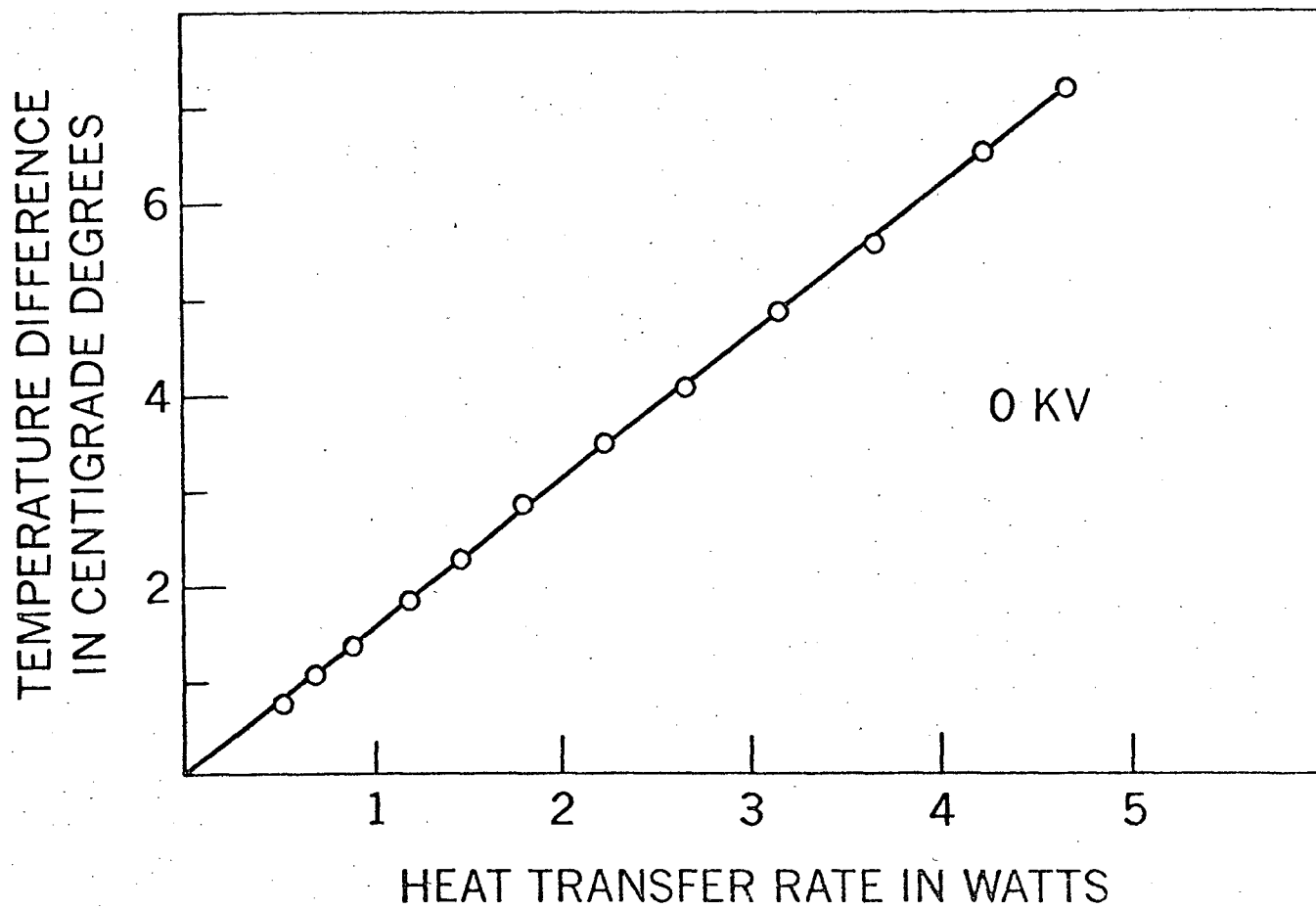


FIGURE 15. DEPENDENCE OF TEMPERATURE DIFFERENCE ON HEAT TRANSFER RATE FOR 0 KV RMS BETWEEN THE CYLINDERS.

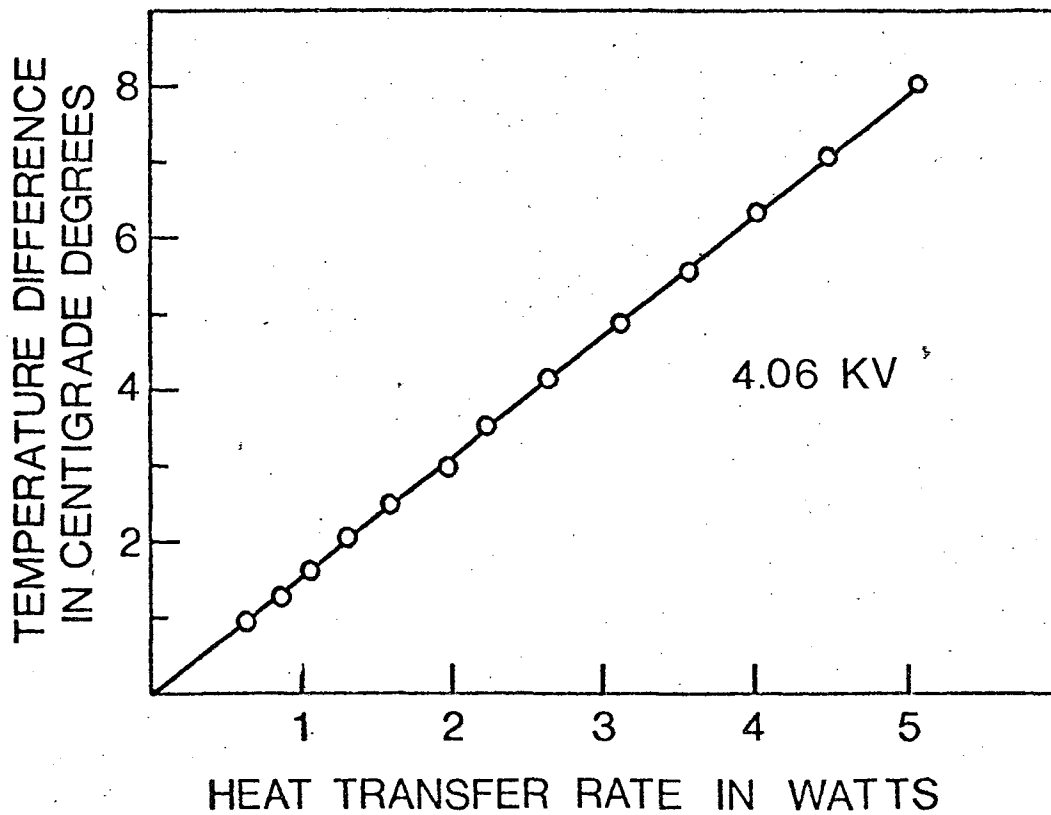


FIGURE 16. DEPENDENCE OF TEMPERATURE DIFFERENCE ON HEAT TRANSFER RATE FOR 4.06 KV RMS BETWEEN THE CYLINDERS.

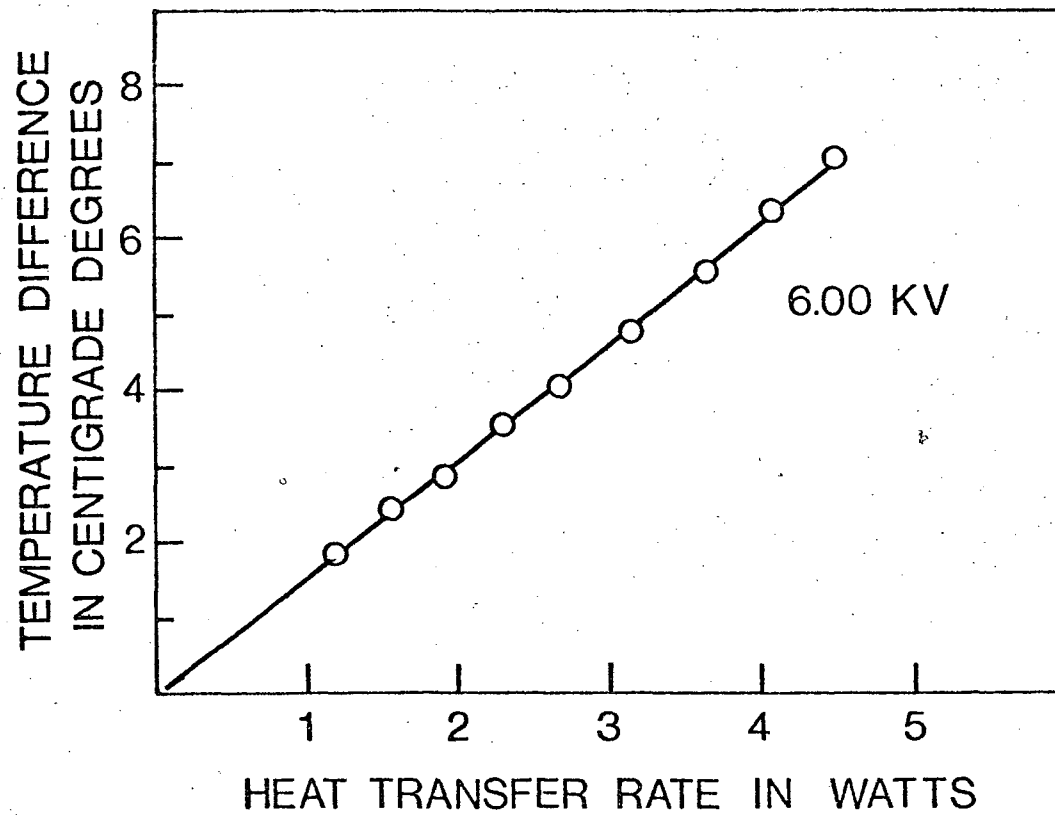


FIGURE 17. DEPENDENCE OF TEMPERATURE DIFFERENCE ON HEAT TRANSFER RATE FOR 6.00 KV RMS BETWEEN THE CYLINDERS.

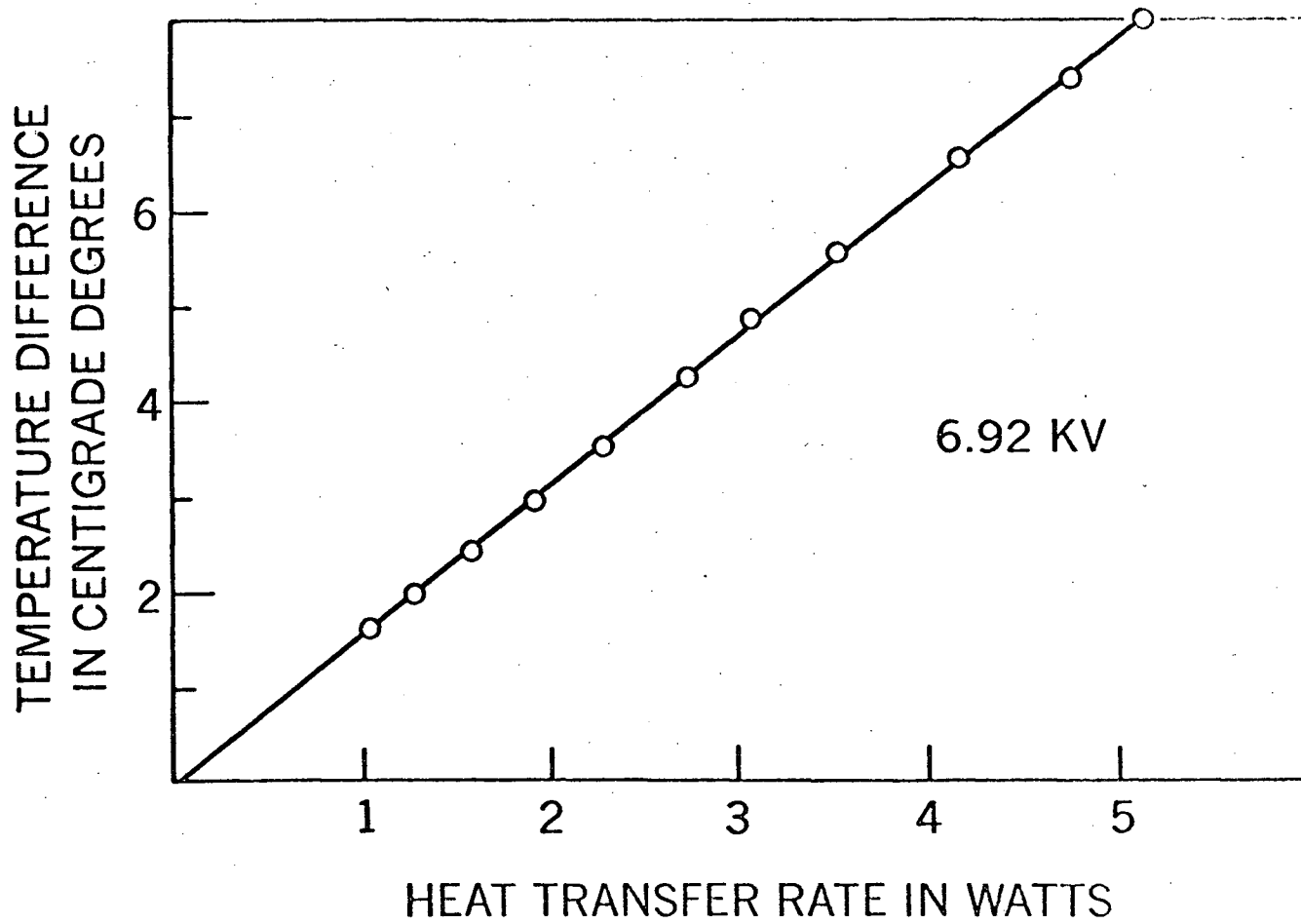


FIGURE 18. DEPENDENCE OF TEMPERATURE DIFFERENCE ON HEAT TRANSFER RATE FOR 6.92 KV RMS BETWEEN THE CYLINDERS.

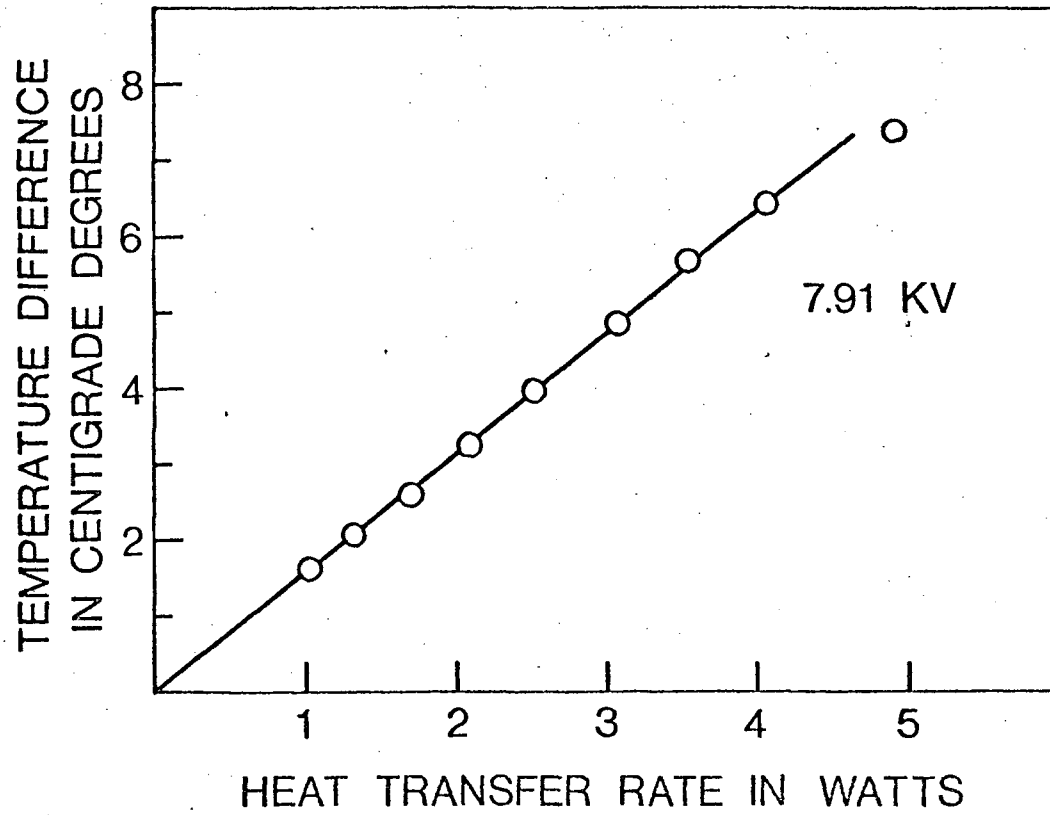


FIGURE 19. DEPENDENCE OF TEMPERATURE DIFFERENCE ON HEAT TRANSFER RATE FOR 7.91 KV RMS BETWEEN THE CYLINDERS.

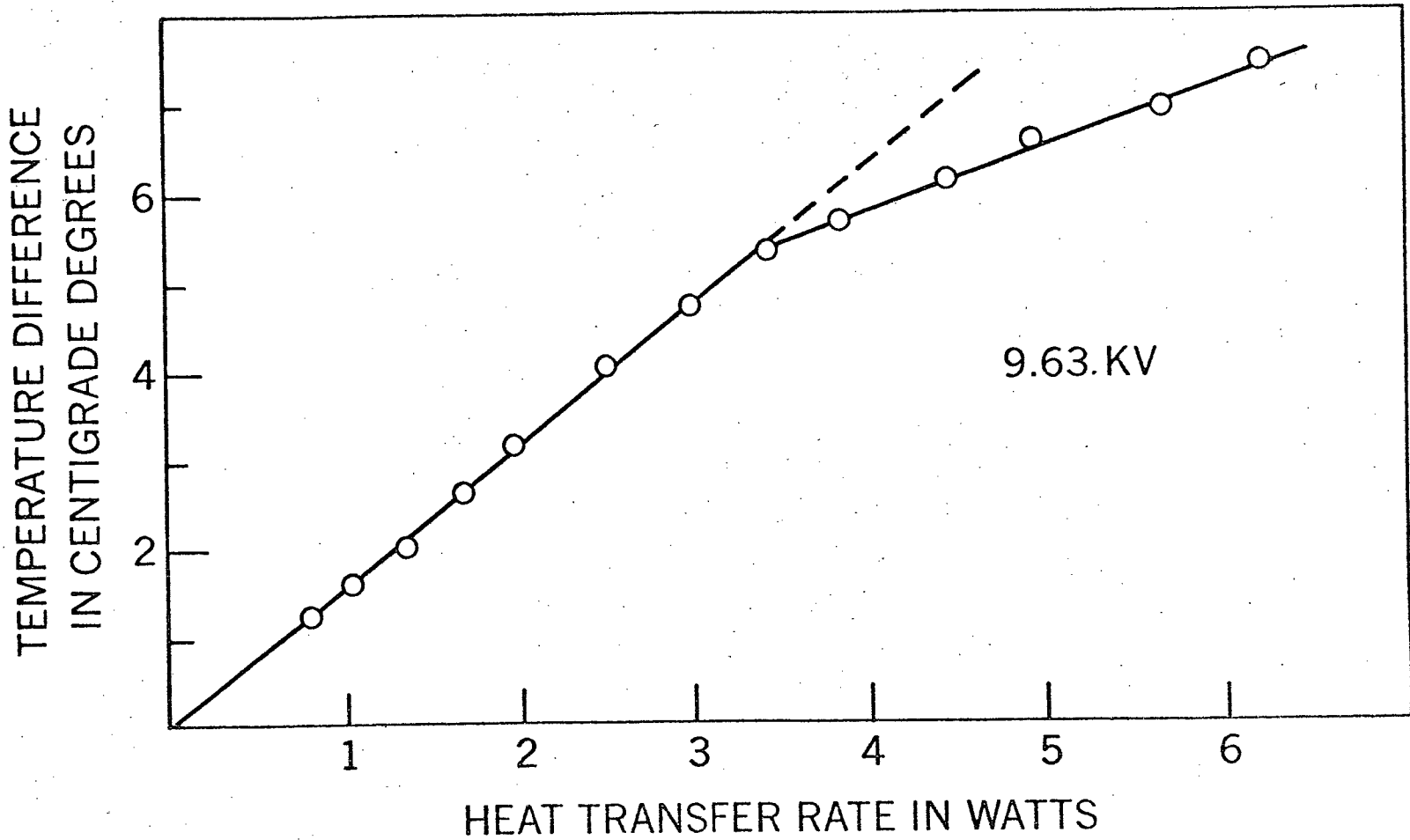


FIGURE 20. DEPENDENCE OF TEMPERATURE DIFFERENCE ON HEAT TRANSFER RATE FOR 9.63 KV RMS BETWEEN THE CYLINDERS.

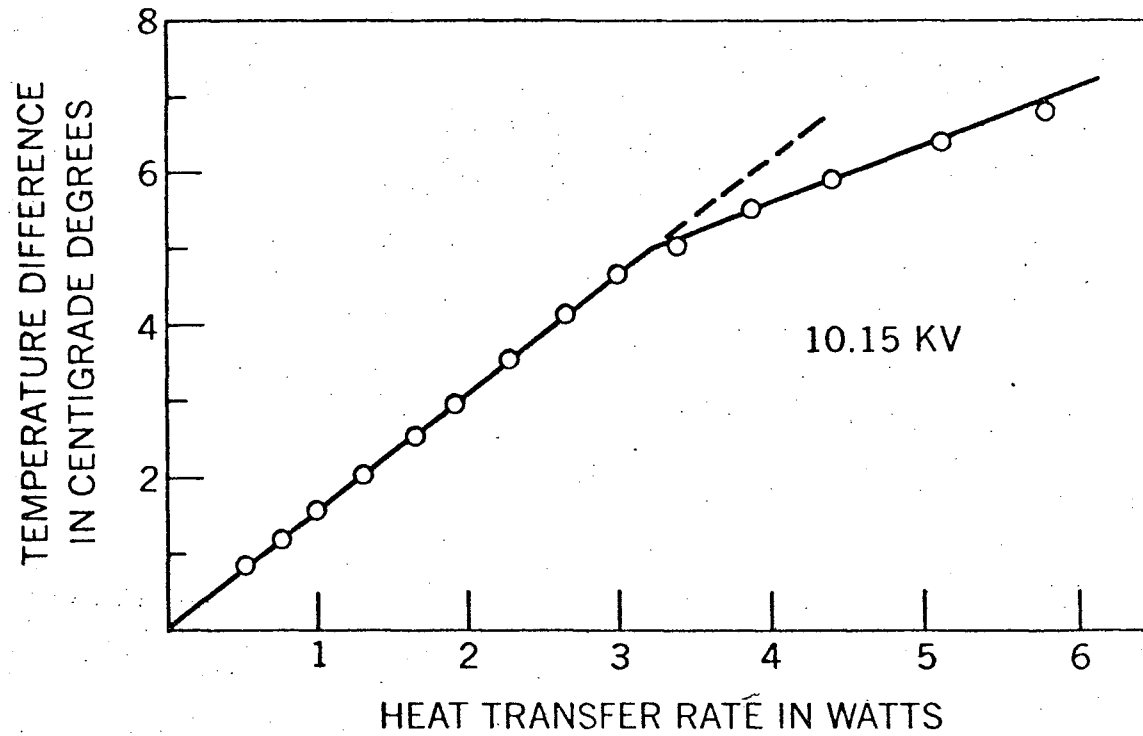


FIGURE 21. DEPENDENCE OF TEMPERATURE DIFFERENCE ON HEAT TRANSFER RATE FOR 10.15 KV RMS BETWEEN THE CYLINDERS.

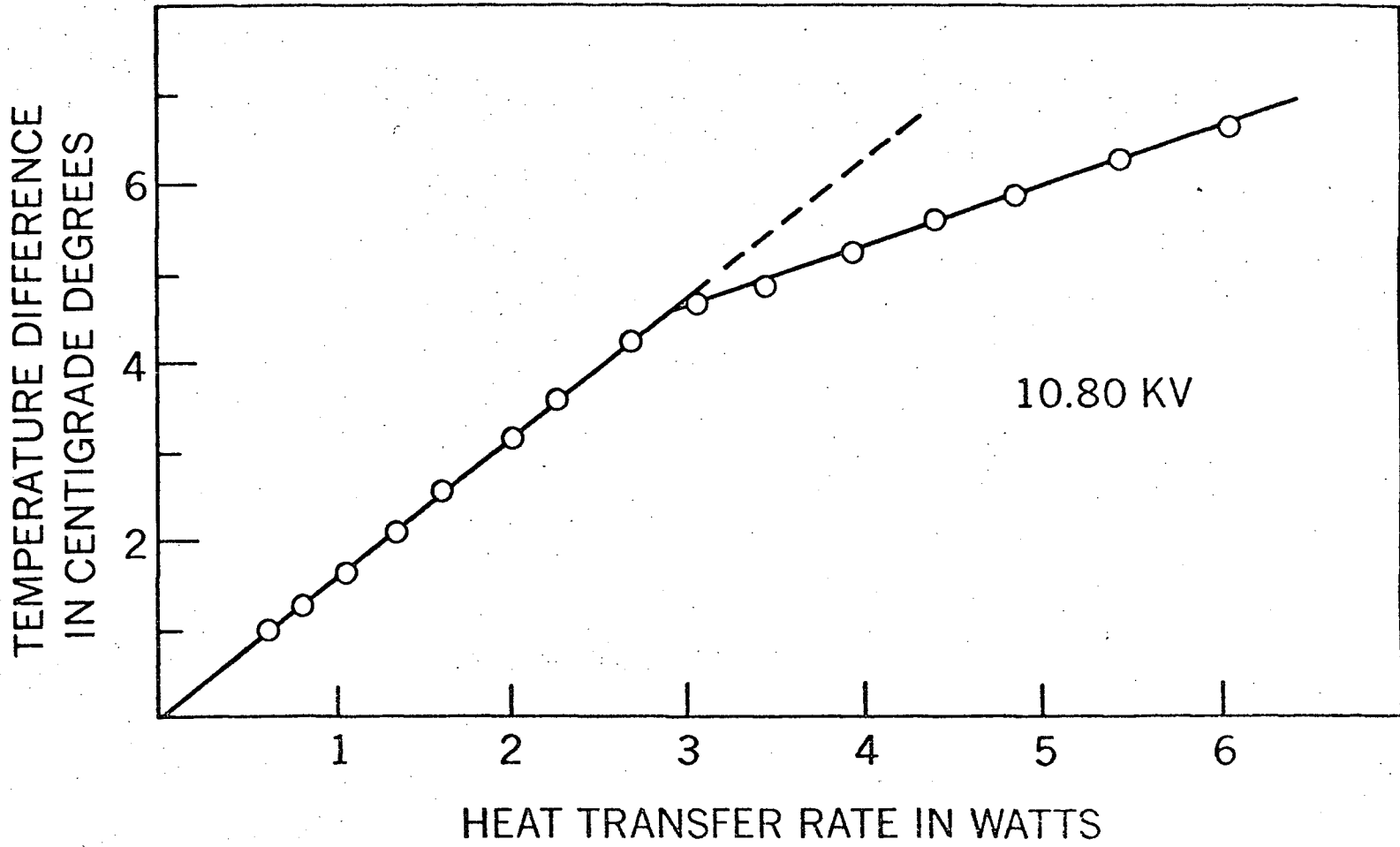


FIGURE 22. DEPENDENCE OF TEMPERATURE DIFFERENCE ON HEAT TRANSFER RATE FOR 10.80 KV RMS BETWEEN THE CYLINDERS.

A bridge voltage of 0.5 volts was used for the resistance measurements which reduced the error due to self-heating far below the required precision.

Error due to finite thickness of walls of the cylinders: The temperature of the inner cylinder was measured by the thermistors mounted on the inner wall. The temperatures of the outer cylinder were those at the outer surface. For any true calculation of conductive heat transfer through the liquid, it is essential to correct for the finite wall thicknesses. The thicknesses of the walls were sufficiently small that it was estimated that the maximum error introduced is less than 0.5% and it was not considered necessary to make this correction.

Errors due to internal resistance of I_1 , I_2 and V_1 : The sensitivity of the voltmeter V_1 , was $20,000\Omega/\text{volt}$. The resistance of the ammeters was 0.1Ω on 1A range compared to about 13Ω for the mid-section of the heating coil. It was, therefore, found unnecessary to do any corrections for the internal resistance of the meters.

3.5 Experimental Results.

Experimental results in the form of the temperature difference between the cylinders plotted against the heat transfer rate in the central section of the annulus are shown in figures 15 through 22 for the range of voltages applied to the outer cylinder. For potentials up to 7.91 kv rms, the relations are linear, indicating

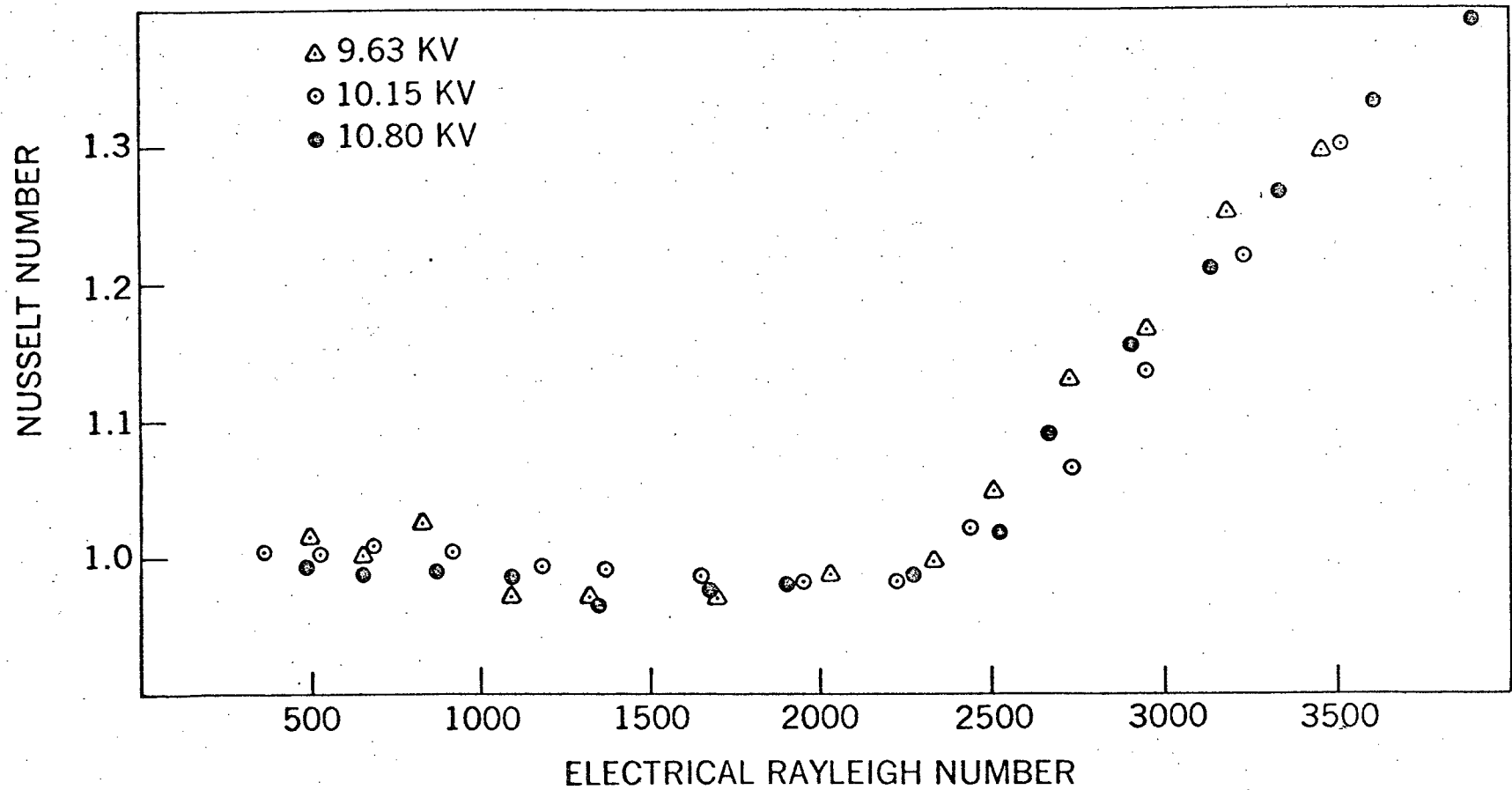


FIGURE 23. NUSSLETT NUMBER AS A FUNCTION OF ELECTRICAL RAYLEIGH NUMBER.

conductive heat transfer even for the maximum temperature differences attained. For potentials of 9.63, 10.15 and 10.80 kv rms, distinct breaks occur in the linear relationship indicating the onset of convective heat transfer.

All the results are summarized in figure 23 as a plot of the Nusselt number

$$\text{Nu} = \frac{v_1(i_1 - i_2) \ln(r_2/r_1)}{4.1854 [2\pi\chi L(T_1 - T_2)]}$$

against the electrical Rayleigh number, R (equation 52, Chapter II). In the above equation χ is the thermal conductivity of the fluid and L is the length of the measurement section between the points 8 and 10 (see figure 6). The values of viscosity and dielectric constant entering in the expression for R were taken at the mean of the temperatures of the cylinders. The thermal conductivity depends so slightly on the temperature that its variation with temperature was ignored. Other constants used for the oil are listed in Table 5.

Figure 23 shows the experimentally determined critical electrical Rayleigh number for the onset of instability to be

$$R_c = 2200 \pm 100.$$

3.6 Accuracy

The accuracy of the final results for Nu and R is estimated to be $\pm 5\%$ when all the factors are considered.

CHAPTER IV

DISCUSSIONS AND CONCLUSIONS

4.1 Discussion of Results

The figures 15 to 22 show the plots of the heat transfer rate against the temperature difference between the cylinders for a range of voltages applied to the outer cylinder. For lower voltages the plots are linear, indicating the heat transfer is by conduction alone. Above 7.91 kv rms, however, the plots show distinct breaks which occur at the onset of instability (Schmidt and Milverton, 1935). The electrical buoyancy force for small voltages was not sufficient to overcome thermal and viscous dissipation even for the maximum temperature differences created across the gap. However, if the temperature of the inner cylinder is raised further, we should expect appreciable convective heat transfer even for those voltages.

The plot of the Nusselt number against the electrical Rayleigh number is shown in figure 23. In the conduction regime, the Nusselt number is found to have a slight downward trend from the expected value of unity. If there is a small temperature drop at the outer wall contact point during the initial run with no high voltage, this could lead to an underestimation of the temperature difference of figure 11. Consequently, the impressed temperature difference between the cylinders would be overestimated. A linear increase of this contact temperature difference with impressed temperature difference could result in a small decrease in the Nusselt number with increasing Rayleigh number.

The value of the electrical Rayleigh number at which the onset of instability occurs is: $R_c = 2200 \pm 100$.

The theoretically determined value of R_c is 2119.346 and compares

well with the experimental value. The disturbances which will be manifested at marginal stability are characterized by the wave length

$$\Lambda = \frac{2\pi}{k} = \frac{2\pi d}{a_c} = 2.02d.$$

The value of a_c for this case is same as for the Rayleigh-Bénard convection ($a_c=3.117$). In the Rayleigh-Bénard instability, the Nusselt number is a function of the Rayleigh number only. Here, however, the Nusselt number depends on the electrical Rayleigh number and the ratio of the inner cylinder radius to gap width.

4.2 Conclusions

The present investigations have demonstrated the feasibility of constructing a laboratory model of thermal convection to simulate large scale geophysical flows that occur under a (nearly) central gravitational field. The marginal stability analysis of the flow was done by making several simplifying assumptions. The general validity of the principle of exchange of stabilities could not be proved for this problem. However, the quality of the agreement of the experimental results with the numerically determined value (assuming the principle of exchange of stabilities) is a strong verification of the validity of the analysis.

In constructing laboratory models of geophysical flows, we need to proceed to spherical geometry and rotation. We should also be interested in the actual form of the flow pattern as well as the values of various parameters at the onset of convection. All this will require the development of some new techniques, but in principle it now appears possible.

REFERENCES

- Avsec, D. and Luntz, M. 1937, Electricité Et Hydrodynamique - Quelques formes nouvelles des tourbillons electroconvections, C. R. Acad. Sci., Paris, 204, 757.
- Batchelor, G. K., 1954, Heat transfer by free convection across a closed cavity between vertical boundaries at different temperatures, Quart. Appl. Math., 12, 209-33.
- Bénard, H., 1900, Les tourbillons cellulaires dans une nappe liquide, Revue generale des science pures et appliques, 11, 1261-71 and 1309-28.
- Bird, R. B., Stewart, W.B. and Lightfoot, E. N., 1966, Transport phenomena, John Wiley, New York.
- Bullard, E. C. and Gellman, H., 1954, Homogeneous dynamos and terrestrial magnetism, Phil. trans. Roy. Soc., Sr A, 247, 213.
- Chandra, B., 1969, Thermal convection under an axially symmetrical force field, M. Sc. Thesis, University of Western Ontario, London, Canada.
- Chandra, K., 1938, Instability of fluids heated from below, Proc. Roy. Soc. (London), Sr A, 164, 231-42.
- Chandrasekhar, S., 1961, Hydrodynamics and hydromagnetic stability, Oxford Univ. Press.
- Debye, P., 1929, Polar molecules, Chemical catalog company, New York, p27.
- Ford, L. R., 1955, Differential equations, McGraw Hill.
- Fultz, D., 1961, Developments in controlled experiments on large scale geophysical problems, Advances in Geophysics, edited by H. E. Landsberg, 7, 1-103.
- Greenspan, H. P., The theory of rotating fluids, Cambridge.
- Gross, M. J., 1967, Laboratory analogies for convection problems, Mantles of the earth and terrestrial planets, edited by S. K. Runcorn, Interscience, 499-503.

- Gross, M. J. and Porter, J. E., 1966, Electrically induced convection in dielectric liquids, *Nature*, no. 5058, 1343-45.
- Hadley, G., 1735, Concerning the cause of the general trade winds, Reprinted in the *Mechanics of the Earth's atmosphere*, Smithsonian Inst. Misc. Coll., 51, no. 4, 1910.
- Ince, E. L., 1956, *Ordinary differential equations*, Dover Publications.
- Jeffreys, H., 1926, The instability of a layer of fluid heated below, *Phil. Mag.*, A, 2, 833-44.
- Kronig, R. and Schwarz, N., 1949, On the theory of heat transfer from a wire in an electric field, *Appl. Sci. Res.*, A1, 35-45.
- Landau, L. D. and Lifshitz, E. M., 1960, *Electrodynamics of continuous media*, Pergamon press, London.
- Long, R. R. (editor), 1955, Fluid models in geophysics, Proc. 1st symposium on the use of models in geophysical fluid dynamics, Balt.
- Low, A. R., 1929, On the criterion for the stability of a layer of viscous fluid heated below, *Proc. Roy. Soc.*, A, 125, 180-95.
- Malkus, W. V. R. and Veronis, G., 1961, Surface electroconvection, *Phys. Fluids*, 4, 13-23.
- Mathews, J. and Walker, R. L., 1964, *Mathematical methods in Physics*, W. A. Benjamin, Inc., New York.
- Melcher, J. R. and Taylor, G. I., 1969, Electrohydrodynamics: A review of the role of interfacial shear stresses, *Annual Review of Fluid Mechanics* edited by W. R. Sears and M. Van Dyke, 1, 111-47.
- McFadden, C. P., 1969, The effect of region of low viscosity on thermal convection in the Earth's mantle, Ph. D. thesis, University of Western Ontario, London, Canada.
- Pellew, A. and Southwell, R. V., 1940, On maintained convective motion in a fluid heated from below, *Proc. Roy. Soc.*, A, 176, 312-43.

- Rayleigh, Lord, 1916, On convective currents in a horizontal layer of fluid when the higher temperature is on the underside, *Phil. Mag.*, 6, 529-46.
- Rossby, C. G., 1941, The scientific basis of modern meteorology, *Yearbook of Agriculture*, U. S. Dept. of Agriculture, 599-655.
- Schmidt, R. J. and Milverton, S. W., 1935, On the instability of a fluid when heated from below, *Proc. Roy. Soc. (London)*, A, 152, 586-94.
- Silveston, P. L., 1958, Wärmedurchgang in Waagerechten Flüssigkeitsschichten, part 1, *Forsch. Ing. Wes.*, 24, 29-32 and 59-69.
- Smylie, D. E., 1966, Thermal convection in dielectric liquids and modelling in geophysical fluid dynamics, *Earth and Planetary Science Letters*, 1, 339-40.
- Turnbull, R. J., 1968, Electroconvective instability with a stabilizing temperature gradient, *Phys. Fluids*, 11, 2588-96 and 2597-2603.
- Vening-Meinesz, F. A., 1962, Thermal convection in the Earth's mantle, *Continental Drift* edited by S. K. Runcorn, Academic Press.
- Vest, C. M. and Arpaci, V. S., 1969, Stability of natural convection in a vertical slot, *J. Fluid Mech.*, 36, 1-16.

APPENDIX I

TABLES OF THERMISTOR CALIBRATION

TABLE NO. 3

TABLE OF CALIBRATION POINTS FOR THERMISTORS ON THE INNER CYLINDER.

	(1)	(2)	(3)
TEMPERATURE DEGREES C	RESISTANCE OHMS	RESISTANCE OHMS	RESISTANCE OHMS
15.037	79912	78088	72127
17.714	70364	68559	63517
20.450	61923	60155	55902
23.166	54671	52952	49352
25.898	48310	46668	43625
28.646	42779	41194	38614

DIFFERENCE BETWEEN CALIBRATED RESISTANCE AND COMPUTED RESISTANCE.

	(1)	(2)	(3)
TEMPERATURE DEGREES C	RESISTANCE OHMS	RESISTANCE OHMS	RESISTANCE OHMS
15.037	-0.81	0.25	1.13
17.714	-0.88	-0.25	-1.40
20.450	0.67	-0.96	-0.86
23.166	6.42	2.98	1.39
25.898	-7.42	-2.51	0.24
28.646	4.10	0.74	-0.36

- (1) THERMISTOR AT POINT 8 ON THE INNER CYLINDER.
 (2) THERMISTOR AT POINT 9 ON THE INNER CYLINDER.
 (3) THERMISTOR AT POINT 10 ON THE INNER CYLINDER.

TABLE NO. 4

TABLE OF CALIBRATION POINTS FOR INLET AND OUTLET POINT THERMISTORS.

TEMPERATURE DEGREES C	(1)	(2)
	RESISTANCE OHMS	RESISTANCE OHMS
11.914	90481	79097
13.868	82165	71816
15.824	74697	65283
17.742	68104	59505
19.677	62082	54242
21.624	56632	49466

DIFFERENCE BETWEEN CALIBRATED RESISTANCE AND COMPUTED RESISTANCE.

TEMPERATURE DEGREES C	(1)	(2)
	RESISTANCE OHMS	RESISTANCE OHMS
11.914	3.44	3.69
13.868	-6.63	-5.25
15.824	-0.44	2.06
17.742	7.06	2.70
19.677	-4.19	-0.46
21.624	0.88	-0.53

(1) THERMISTOR AT POINT 11 AT THE INLET POINT TO THE THERMAL FLASK.

(2) THERMISTOR AT POINT 12 AT THE OUTLET POINT TO THE THERMAL FLASK.

APPENDIX II

TABLES OF HEAT TRANSFER MEASUREMENTS

TABLE NO. 6

VOLTAGE BETWEEN THE CYLINDERS= 0.0 KV

(1)	(2)	(3)	(4)	(5)	(6)	(7)	(8)
16.34	16.35	16.35	16.61	16.82	0.0	0.0	0.0
17.58	17.57	17.57	16.61	16.78	0.263	0.073	2.57
18.02	18.01	18.00	16.59	16.73	0.304	0.084	2.98
18.49	18.50	18.49	16.61	16.80	0.349	0.096	3.42
19.29	19.28	19.28	16.62	16.82	0.402	0.108	3.98
20.01	20.00	20.00	16.63	16.78	0.446	0.118	4.45
20.89	20.88	20.88	16.62	16.78	0.496	0.132	4.95
21.91	21.90	21.89	16.64	16.79	0.543	0.138	5.48
22.98	22.97	22.97	16.60	16.74	0.596	0.154	6.02
24.13	24.13	24.13	16.60	16.74	0.643	0.162	6.55
25.45	25.45	25.45	16.73	16.83	0.698	0.177	7.05
26.78	26.77	26.78	16.65	16.79	0.749	0.189	7.58
27.82	27.82	27.83	16.64	16.80	0.787	0.201	7.97

- (1) TEMPERATURE OF INNER CYLINDER AT POINT 10.
(2) TEMPERATURE OF INNER CYLINDER AT POINT 9.
(3) TEMPERATURE OF INNER CYLINDER AT POINT 8.
(4) TEMPERATURE OF CIRCULATING OIL AT INLET POINT 11.
(5) TEMPERATURE OF CIRCULATING OIL AT OUTLET POINT 12.
(6) CURRENT I1 IN AMPERES.
(7) CURRENT I2 IN AMPERES.
(8) VOLTAGE V1 IN VOLTS.

TABLE NO. 7

VOLTAGE BETWEEN THE CYLINDERS = 4.06KV

(1)	(2)	(3)	(4)	(5)	(6)	(7)	(8)
17.88	17.89	17.88	16.65	16.85	0.303	0.088	2.90
18.41	18.42	18.42	16.62	16.80	0.353	0.113	3.50
19.03	19.03	19.02	16.64	16.86	0.402	0.124	3.74
19.68	19.68	19.67	16.65	16.83	0.450	0.141	4.18
20.47	20.47	20.47	16.71	16.89	0.502	0.160	4.65
21.23	21.23	21.23	16.70	16.86	0.547	0.174	5.33
22.17	22.16	22.17	16.67	16.91	0.594	0.189	5.50
23.23	23.23	23.24	16.82	17.11	0.644	0.202	5.96
24.37	24.38	24.37	16.79	17.06	0.700	0.220	6.50
25.51	25.51	25.49	16.74	16.92	0.750	0.236	6.95
26.70	26.70	26.69	16.76	16.98	0.801	0.255	7.41
27.83	27.82	27.82	16.76	17.01	0.845	0.268	7.81
29.33	29.33	29.34	16.78	17.02	0.898	0.286	8.37

- (1) TEMPERATURE OF INNER CYLINDER AT POINT 10.
(2) TEMPERATURE OF INNER CYLINDER AT POINT 9.
(3) TEMPERATURE OF INNER CYLINDER AT POINT 8.
(4) TEMPERATURE OF CIRCULATING OIL AT INLET POINT 11.
(5) TEMPERATURE OF CIRCULATING OIL AT OUTLET POINT 12.
(6) CURRENT I1 IN AMPERES.
(7) CURRENT I2 IN AMPERES.
(8) VOLTAGE V1 IN VOLTS.

TABLE NO. 8

VOLTAGE BETWEEN THE CYLINDERS= 6.00KV

(1)	(2)	(3)	(4)	(5)	(6)	(7)	(8)
19.49	19.50	19.50	16.86	17.08	0.437	0.139	4.03
20.44	20.45	20.45	16.80	17.02	0.496	0.156	4.61
21.36	21.37	21.37	16.87	17.15	0.552	0.174	5.13
22.35	22.35	22.34	16.87	17.16	0.602	0.189	5.58
23.26	23.26	23.25	16.89	17.21	0.649	0.204	6.02
24.30	24.29	24.30	16.89	17.19	0.701	0.218	6.54
25.54	25.55	25.53	16.84	17.12	0.763	0.243	7.04
26.78	26.79	26.77	16.85	17.12	0.801	0.253	7.45
27.91	27.90	27.90	16.83	17.04	0.848	0.273	7.85

- (1) TEMPERATURE OF INNER CYLINDER AT POINT 10.
(2) TEMPERATURE OF INNER CYLINDER AT POINT 9.
(3) TEMPERATURE OF INNER CYLINDER AT POINT 8.
(4) TEMPERATURE OF CIRCULATING OIL AT INLET POINT 11.
(5) TEMPERATURE OF CIRCULATING OIL AT OUTLET POINT 12.
(6) CURRENT I1 IN AMPERES.
(7) CURRENT I2 IN AMPERES.
(8) VOLTAGE V1 IN VOLTS.

TABLE NO. 9

VOLTAGE BETWEEN THE CYLINDERS = 6.92KV

(1)	(2)	(3)	(4)	(5)	(6)	(7)	(8)
19.05	19.05	19.06	16.70	17.02	0.404	0.126	3.75
19.67	19.67	19.67	16.74	17.00	0.448	0.141	4.17
20.44	20.44	20.43	16.71	17.08	0.499	0.157	4.63
21.28	21.28	21.26	16.75	17.04	0.547	0.173	5.08
22.25	22.25	22.24	16.79	17.06	0.600	0.189	5.57
23.30	23.30	23.30	16.73	16.99	0.654	0.206	6.07
24.22	24.21	24.21	16.68	16.98	0.700	0.224	6.44
25.33	25.33	25.33	16.72	16.97	0.747	0.231	6.84
26.91	26.92	26.91	16.72	16.98	0.816	0.261	7.54
28.38	28.38	28.38	16.72	16.96	0.871	0.275	8.10
29.43	29.44	29.44	16.72	16.96	0.917	0.291	8.50

- (1) TEMPERATURE OF INNER CYLINDER AT POINT 10.
(2) TEMPERATURE OF INNER CYLINDER AT POINT 9.
(3) TEMPERATURE OF INNER CYLINDER AT POINT 8.
(4) TEMPERATURE OF CIRCULATING OIL AT INLET POINT 11.
(5) TEMPERATURE OF CIRCULATING OIL AT OUTLET POINT 12.
(6) CURRENT I1 IN AMPERES.
(7) CURRENT I2 IN AMPERES.
(8) VOLTAGE V1 IN VOLTS.

TABLE NO. 10

VOLTAGE BETWEEN THE CYLINDERS= 7.91KV

(1)	(2)	(3)	(4)	(5)	(6)	(7)	(8)
19.04	19.04	19.04	16.66	16.92	0.402	0.128	3.72
19.75	19.75	19.75	16.67	16.89	0.452	0.139	4.23
20.62	20.62	20.61	16.70	16.86	0.509	0.155	4.78
21.67	21.68	21.67	16.68	16.90	0.560	0.168	5.32
22.83	22.82	22.82	16.67	16.92	0.627	0.196	5.83
24.22	24.23	24.23	16.71	16.95	0.700	0.224	6.43
25.57	25.57	25.57	16.74	16.94	0.769	0.252	6.98
26.68	26.67	26.67	16.69	16.92	0.828	0.279	7.44
28.30	28.30	28.30	16.64	16.82	0.895	0.291	8.20

- (1) TEMPERATURE OF INNER CYLINDER AT POINT 10.
 (2) TEMPERATURE OF INNER CYLINDER AT POINT 9.
 (3) TEMPERATURE OF INNER CYLINDER AT POINT 8.
 (4) TEMPERATURE OF CIRCULATING OIL AT INLET POINT 11.
 (5) TEMPERATURE OF CIRCULATING OIL AT CUTLET POINT 12.
 (6) CURRENT I1 IN AMPERES.
 (7) CURRENT I2 IN AMPERES.
 (8) VOLTAGE V1 IN VOLTS.

TABLE NO. 11

VOLTAGE BETWEEN THE CYLINDERS= 9.63KV

(1)	(2)	(3)	(4)	(5)	(6)	(7)	(8)
18.41	18.42	18.43	16.71	16.83	0.351	0.10P	3.26
19.05	19.06	19.06	16.69	16.89	0.402	0.125	3.73
19.74	19.75	19.74	16.65	16.89	0.453	0.144	4.20
20.66	20.66	20.65	16.59	16.89	0.517	0.166	4.77
21.52	21.52	21.51	16.66	16.88	0.569	0.187	5.18
22.85	22.84	22.84	16.69	16.86	0.643	0.213	5.83
23.98	23.97	23.97	16.69	16.86	0.707	0.235	6.38
24.91	24.91	24.91	16.68	16.88	0.757	0.250	6.85
25.69	25.70	25.70	16.67	16.81	0.800	0.264	7.25
26.68	26.68	26.68	16.65	16.85	0.855	0.279	7.82
27.53	27.52	27.52	16.63	16.81	0.898	0.293	8.24
28.72	28.72	28.73	16.71	17.01	0.953	0.300	8.84
29.65	29.65	29.66	16.71	16.85	0.998	0.312	9.94

- (1) TEMPERATURE OF INNER CYLINDER AT POINT 10.
(2) TEMPERATURE OF INNER CYLINDER AT POINT 9.
(3) TEMPERATURE OF INNER CYLINDER AT POINT 8.
(4) TEMPERATURE OF CIRCULATING OIL AT INLET POINT 11.
(5) TEMPERATURE OF CIRCULATING OIL AT OUTLET POINT 12.
(6) CURRENT I1 IN AMPERES.
(7) CURRENT I2 IN AMPERES.
(8) VOLTAGE V1 IN VOLTS.

TABLE NO. 12

VOLTAGE BETWEEN THE CYLINDERS= 10.15KV

(1)	(2)	(3)	(4)	(5)	(6)	(7)	(8)
17.74	17.75	17.75	16.67	16.82	0.287	0.088	2.64
18.35	18.35	18.36	16.66	16.88	0.341	0.103	3.20
18.92	18.92	18.92	16.69	16.82	0.391	0.119	3.65
19.70	19.71	19.71	16.68	16.85	0.449	0.138	4.21
20.55	20.56	20.55	16.69	16.83	0.507	0.161	4.70
21.21	21.20	21.20	16.67	16.86	0.550	0.171	5.02
22.12	22.13	22.12	16.70	16.88	0.611	0.198	5.47
23.01	23.01	23.00	16.65	16.83	0.661	0.215	5.93
23.83	23.83	23.82	16.63	16.80	0.700	0.231	6.35
24.62	24.62	24.62	16.63	16.89	0.744	0.246	6.77
25.57	25.57	25.57	16.66	16.79	0.800	0.264	7.25
26.43	26.42	26.42	16.65	16.79	0.851	0.281	7.75
27.39	27.39	27.39	16.65	16.79	0.911	0.291	8.28
28.47	28.46	28.47	16.66	16.80	0.950	0.294	8.85

- (1) TEMPERATURE OF INNER CYLINDER AT POINT 10.
(2) TEMPERATURE OF INNER CYLINDER AT POINT 9.
(3) TEMPERATURE OF INNER CYLINDER AT POINT 8.
(4) TEMPERATURE OF CIRCULATING OIL AT INLET POINT 11.
(5) TEMPERATURE OF CIRCULATING OIL AT OUTLET POINT 12.
(6) CURRENT I1 IN AMPERES.
(7) CURRENT I2 IN AMPERES.
(8) VOLTAGE V1 IN VOLTS.

TABLE NO. 13

VOLTAGE BETWEEN THE CYLINDERS= 10.80KV

(1)	(2)	(3)	(4)	(5)	(6)	(7)	(8)
17.94	17.95	17.95	16.66	16.76	0.310	0.095	2.88
18.41	18.42	18.42	16.61	16.77	0.354	0.108	3.30
19.09	19.10	19.09	16.59	16.77	0.408	0.126	3.80
19.77	19.77	19.77	16.66	16.78	0.462	0.147	4.27
20.45	20.45	20.44	16.60	16.76	0.505	0.161	4.68
21.44	21.44	21.43	16.61	16.77	0.568	0.181	5.20
22.14	22.14	22.14	16.61	16.71	0.607	0.197	5.55
23.10	23.10	23.10	16.61	16.76	0.662	0.216	6.05
23.83	23.83	23.82	16.57	16.68	0.707	0.230	6.45
24.49	24.49	24.50	16.66	16.82	0.752	0.245	6.85
25.35	25.34	25.34	16.66	16.78	0.792	0.251	7.34
26.10	26.10	26.10	16.65	16.77	0.830	0.257	7.75
26.80	26.80	26.81	16.65	16.80	0.869	0.267	8.14
27.76	27.77	27.77	16.67	16.76	0.919	0.283	8.63
28.72	28.72	28.72	16.62	16.81	0.975	0.298	9.06

- (1) TEMPERATURE OF INNER CYLINDER AT POINT 10.
(2) TEMPERATURE OF INNER CYLINDER AT POINT 9.
(3) TEMPERATURE OF INNER CYLINDER AT POINT 8.
(4) TEMPERATURE OF CIRCULATING OIL AT INLET POINT 11.
(5) TEMPERATURE OF CIRCULATING OIL AT OUTLET POINT 12.
(6) CURRENT I1 IN AMPERES.
(7) CURRENT I2 IN AMPERES.
(8) VOLTAGE V1 IN VOLTS.

APPENDIX III

TABLES OF CORRECTED DATA

TABLE NO 14

VOLTAGE BETWEEN THE CYLINDERS= 0.0 KV

(1)	(2)	(3)	(4)	(5)
16.35	16.36	0.0	0.0	0.0
17.57	16.82	0.2658	0.0742	2.611
18.01	16.98	0.3078	0.0858	3.030
18.49	17.17	0.3524	0.0980	3.462
19.28	17.48	0.4048	0.1100	4.000
20.00	17.75	0.4487	0.1200	4.466
20.88	18.06	0.4986	0.1340	4.952
21.90	18.45	0.5446	0.1400	5.510
22.97	18.95	0.5966	0.1556	6.049
24.13	19.31	0.6430	0.1638	6.568
25.45	19.93	0.6974	0.1785	7.058
26.78	20.29	0.7482	0.1902	7.584
27.82	20.70	0.7860	0.2019	7.971

(1) MEAN TEMPERATURE OF INNER CYLINDER.

(2) MEAN TEMPERATURE OF OUTER CYLINDER.

(3) CORRECTED I1.

(4) CORRECTED I2.

(5) CORRECTED V1.

TABLE NO 15

VOLTAGE BETWEEN THE CYLINDERS= 4.06 KV

(1)	(2)	(3)	(4)	(5)
17.88	16.94	0.3068	0.0898	2.947
18.42	17.15	0.3561	0.1150	3.540
19.03	17.42	0.4048	0.1260	3.770
19.68	17.64	0.4527	0.1430	4.199
20.47	17.98	0.5044	0.1617	4.661
21.23	18.29	0.5485	0.1755	5.330
22.17	18.67	0.5947	0.1902	5.530
23.23	19.11	0.6440	0.2029	5.990
24.37	19.51	0.6994	0.2206	6.520
25.50	19.94	0.7493	0.2365	6.962
26.70	20.32	0.8000	0.2553	7.415
27.82	20.76	0.8432	0.2684	7.812
29.33	21.32	0.8952	0.2864	8.370

- (1) MEAN TEMPERATURE OF INNER CYLINDER.
(2) MEAN TEMPERATURE OF OUTER CYLINDER.
(3) CORRECTED I1.
(4) CORRECTED I2.
(5) CORRECTED V1.

TABLE NO 16

VOLTAGE BETWEEN THE CYLINDERS= 6.00 KV

(1)	(2)	(3)	(4)	(5)
19.50	17.69	0.4398	0.1410	4.049
20.45	18.05	0.4985	0.1578	4.622
21.37	18.51	0.5534	0.1755	5.160
22.35	18.84	0.6024	0.1902	5.610
23.26	19.23	0.5490	0.2049	6.048
24.30	19.65	0.7003	0.2187	6.559
25.54	20.03	0.7622	0.2433	7.048
26.78	20.44	0.7999	0.2533	7.455
27.90	20.82	0.8463	0.2733	7.851

- (1) MEAN TEMPERATURE OF INNER CYLINDER.
(2) MEAN TEMPERATURE OF OUTER CYLINDER.
(3) CORRECTED I1.
(4) CORRECTED I2.
(5) CORRECTED V1.

TABLE NO 17

VOLTAGE BETWEEN THE CYLINDERS= 6.92 KV

(1)	(2)	(3)	(4)	(5)
19.05	17.48	0.4068	0.1280	3.780
19.67	17.74	0.4506	0.1430	4.188
20.44	18.04	0.5014	0.1588	4.642
21.28	18.35	0.5484	0.1746	5.110
22.25	18.75	0.6004	0.1902	5.600
23.30	19.08	0.6539	0.2069	6.097
24.21	19.36	0.6994	0.2246	6.461
25.33	19.81	0.7463	0.2316	6.852
26.91	20.40	0.8142	0.2613	7.544
28.38	21.07	0.8684	0.2753	8.100
29.44	21.49	0.9128	0.2913	8.500

- (1) MEAN TEMPERATURE OF INNER CYLINDER.
(2) MEAN TEMPERATURE OF OUTER CYLINDER.
(3) CORRECTED I1.
(4) CORRECTED I2.
(5) CORRECTED V1.

TABLE NO 18

VOLTAGE BETWEEN THE CYLINDERS= 7.91 KV

(1)	(2)	(3)	(4)	(5)
19.04	17.43	0.4049	0.1300	3.747
19.75	17.69	0.4546	0.1410	4.247
20.62	18.03	0.5112	0.1568	4.788
21.67	18.43	0.5613	0.1697	5.350
22.82	18.90	0.6271	0.1971	5.860
24.23	19.41	0.6996	0.2246	6.452
25.57	19.88	0.7682	0.2523	6.990
26.67	20.27	0.8267	0.2793	7.445
28.30	20.95	0.8922	0.2913	8.200

- (1) MEAN TEMPERATURE OF INNER CYLINDER.
(2) MEAN TEMPERATURE OF OUTER CYLINDER.
(3) CORRECTED I1.
(4) CORRECTED I2.
(5) CORRECTED V1.

TABLE NO 19

VOLTAGE BETWEEN THE CYLINDERS= 9.63 KV

(1)	(2)	(3)	(4)	(5)
18.42	17.20	0.3544	0.1100	3.307
19.06	17.45	0.4049	0.1270	3.760
19.73	17.73	0.4557	0.1460	4.390
20.66	18.02	0.5191	0.1677	4.777
21.52	18.37	0.5701	0.1883	5.210
22.84	18.88	0.6430	0.2137	5.860
23.97	19.27	0.7063	0.2356	6.404
24.91	19.58	0.7562	0.2503	6.863
25.70	20.03	0.7990	0.2643	7.257
26.68	20.59	0.8530	0.2793	7.822
27.52	21.00	0.8952	0.2933	8.240
28.72	21.82	0.9493	0.3058	8.840
29.65	22.26	0.9980	0.3177	9.235

- (1) MEAN TEMPERATURE OF INNER CYLINDER.
(2) MEAN TEMPERATURE OF OUTER CYLINDER.
(3) CORRECTED I1.
(4) CORRECTED I2.
(5) CORRECTED V1.

TABLE NO 20

VOLTAGE BETWEEN THE CYLINDERS= 10.15 KV

(1)	(2)	(3)	(4)	(5)
17.75	16.93	0.2906	0.0898	2.682
18.35	17.17	0.3436	0.1050	3.246
18.92	17.39	0.3941	0.1210	3.683
19.71	17.70	0.4517	0.1400	4.228
20.55	17.99	0.5093	0.1628	4.790
21.20	18.24	0.5514	0.1724	5.050
22.12	18.60	0.6116	0.1190	5.500
23.01	18.88	0.6610	0.2157	5.942
23.83	19.18	0.6994	0.2316	6.373
24.62	19.57	0.7432	0.2464	6.784
25.57	19.99	0.7990	0.2643	7.257
26.42	20.48	0.8490	0.2813	7.752
27.39	21.02	0.9083	0.2913	8.283
28.47	21.67	0.9477	0.2943	8.850

- (1) MEAN TEMPERATURE OF INNER CYLINDER.
(2) MEAN TEMPERATURE OF OUTER CYLINDER.
(3) CORRECTED I1.
(4) CORRECTED I2.
(5) CORRECTED V1.

TABLE NO 21

VOLTAGE BETWEEN THE CYLINDERS= 10.80 KV

(1)	(2)	(3)	(4)	(5)
17.95	16.97	0.3138	0.0968	2.927
18.42	17.15	0.3574	0.1100	3.340
19.09	17.40	0.4109	0.1280	3.828
19.77	17.67	0.4647	0.1490	4.287
20.45	17.87	0.5073	0.1628	4.690
21.44	18.26	0.5692	0.1824	5.230
22.14	18.57	0.6074	0.1980	5.580
23.10	18.89	0.6618	0.2167	6.079
23.83	19.18	0.7064	0.2306	6.472
24.49	19.64	0.7512	0.2454	6.863
25.34	20.08	0.7910	0.2513	7.347
26.10	20.50	0.8284	0.2573	7.753
26.80	20.93	0.8667	0.2573	8.140
27.77	21.48	0.9158	0.2833	8.630
28.72	22.04	0.9710	0.2983	9.058

- (1) MEAN TEMPERATURE OF INNER CYLINDER.
(2) MEAN TEMPERATURE OF OUTER CYLINDER.
(3) CORRECTED I1.
(4) CORRECTED I2.
(5) CORRECTED V1.